TECHNISCHE
UNIVERSITÄT
WIEN
Vienna University of Technology

INSTITUT FÜR
MECHANIK UND
MECHATRONIK
Mechanics & Mechatronics

A MASTER THESIS ON

Predictive Battery Thermal Management Strategy for Heavy-Duty Fuel Cell Electric Trucks

IN PARTIAL FULFILLMENT OF THE REQUIREMENTS
FOR THE DEGREE OF

Diplom-Ingenieur

(Equivalent to Master of Science)

in

Mechanical Engineering (066 445)

by

Zottl Yves, BSc

01425889

Supervisor:

Associate Prof. Dipl.-Ing. Dr.techn. Hametner Christoph

Dott.mag. Dr.techn. Ferrara Alessandro

Institute of Mechanics and Mechatronics

Research Group for Regelungsmethoden-Antriebssysteme

SUBMITTED AT THE TECHNICAL UNIVERSITY VIENNA

Faculty of Mechanical and Industrial Engineering

Vienna, Austria

June 2024

Abstract

Current and future regulations are increasingly pushing to replace fossil fuels with alternative fuels. There are several other methods of energy sources available besides environmentally harmful sources, such as fossil fuels. One possible solution is using fuel cells in combination with a battery pack. This thesis aims to get an overview of how predictive control can be used to keep the temperature of a battery within a specific temperature range. To this end, a model predictive control system is being implemented in a hydrogen fuel cell truck. Typically, fuel cell trucks gain the driving power from two energy sources: fuel cell and battery. The fuel cell is an electrochemical process using hydrogen and oxygen. This outputs the desired electrical power for the drive and, as a by-product, pure water. Thus, this fuel cell truck can be considered emission-free for operation.

The battery energy is used as a backup source when the power demand exceeds the maximum fuel cell power. This happens especially on steeper routes. Another function of the battery includes the recuperated energy during braking to be considered a buffer. An electric powertrain is installed in the truck to control the power distribution in these two systems. This powertrain regulates the energy management in the system and decides automatically when the fuel cell power is not sufficient anymore and transmits the battery energy to the drive.

For this system, there exist some restrictions, especially in the size of the cooling system, because of the limited space in the truck. In order to ensure sufficient cooling for the truck's battery, a model predictive controller is investigated in this thesis. This uses a linear model and constraint for the calculation. A reference target for the battery temperature and soft constraint is implemented for better results to keep the battery temperature close to the desired reference temperature. Higher temperatures lead to accelerated battery degradation, resulting in a shorter lifespan and decreased efficiency. Therefore, cooling must be applied in advance to keep the battery's temperature within a predefined range.

A forecast on the route is used, which contains route information, including elevation and speed limits. With this data, it is possible to forecast the electrical load on the system. In addition, predictive energy management can be used to estimate the ohmic losses. All this information is needed for the MPC, which predicts the desired cooling power of the battery. The result of this study shows a significant improvement in maintaining the battery temperature close to the desired reference temperature under different load requirements. The use of a predictive cooling strategy can, therefore, increase the service life of the battery.

Kurzfassung

Aktuelle und künftige Vorschriften drängen zunehmend darauf, fossile Brennstoffe durch alternative Brennstoffe zu ersetzen. Es gibt mehrere Methoden, um neben umweltschädlichen Quellen wie fossilen Brennstoffen auch andere Energiequellen zu nutzen. Eine mögliche Lösung ist die Verwendung von Brennstoffzellen in Kombination mit einer Batterie. Ziel dieser Arbeit ist es, einen Überblick darüber zu erhalten, wie eine prädiktive Steuerung eingesetzt werden kann, um die Temperatur einer Batterie innerhalb eines bestimmten Temperaturbereichs zu halten. Zu diesem Zweck wird ein modellprädiktives Regelungssystem in einem Wasserstoff-Brennstoffzellen-LKW implementiert. Typischerweise gewinnen diese LKWs die Antriebsenergie aus zwei Energiequellen, aus der Brennstoffzelle und aus einer Batterie. Die Brennstoffzelle ist ein elektrochemischer Prozess, der Wasserstoff und Sauerstoff verwendet. Dieser liefert die gewünschte elektrische Leistung für den Antrieb und als Nebenprodukt reines Wasser. Damit kann dieser FC-LKW als emissionsfrei im Betrieb angesehen werden.

Die Batterieenergie wird als Reservequelle genutzt, wenn der Strombedarf die maximale Brennstoffzellenleistung übersteigt. Dies geschieht vor allem auf steileren Strecken. Eine weitere Funktion der Batterie ist die Rückgewinnung von Energie beim Bremsen, so dass sie als Puffer dienen kann. Ein elektrischer Antriebsstrang ist im LKW installiert, um die Energieverteilung in diesen beiden Systemen zu steuern. Dieser Antriebsstrang regelt das EMS und entscheidet automatisch, wann die Leistung der Brennstoffzelle nicht mehr ausreicht und überträgt die Energie der Batterie an den Antrieb.

Für dieses System gibt es einige Einschränkungen, insbesondere bei der Größe des Kühlsystems, da der Platz im LKW begrenzt ist. Um eine ausreichende Kühlung der LKW-Batterie zu gewährleisten, wird in dieser Arbeit ein MPC untersucht. Dieser verwendet ein lineares Modell und Beschränkungen für die Berechnung. Um bessere Ergebnisse zu erzielen, werden eine Batteriereferenztemperatur und weiche Beschränkungen implementiert, um die Batterietemperatur nahe an der gewünschten Referenztemperatur zu halten. Höhere Temperaturen führen zu einer beschleunigten Degradation der Batterie, was eine kürzere Lebensdauer und eine geringere Effizienz zur Folge hat. Daher muss im Voraus gekühlt werden, um die Temperatur der Batterie in einem vordefinierten Bereich zu halten. Hierfür wird eine Routenvorhersage verwendet, die Streckeninformationen, einschließlich Höhen- und Geschwindigkeitsbegrenzungen, enthält. Mit diesen Daten ist es möglich, die elektrische Belastung des Systems vorherzusagen. Darüber hinaus kann das prädiktive EMS genutzt werden, um die ohmschen Verluste abzuschätzen. All diese Informationen werden für den MPC benötigt, das die gewünschte Kühlleistung der Batterie vorhersagt.

Das Ergebnis dieser Studie zeigt eine deutliche Verbesserung bei der Aufrechterhaltung der Batterietemperatur in der Nähe der gewünschten Referenztemperatur unter verschiedenen Lastanforderungen. Der Einsatz einer prädiktiven Kühlstrategie kann daher die Lebensdauer der Batterie erhöhen.

Erklärung

Hiermit erkläre ich, dass die vorliegende Arbeit ohne unzulässige Hilfe Dritter und ohne Benutzung anderer als der angegebenen Hilfsmittel angefertigt wurde. Die aus anderen Quellen oder indirekt übernommenen Daten und Konzepte sind unter Angabe der Quelle gekennzeichnet.

Die Arbeit wurde bisher weder im In- noch im Ausland in gleicher oder in ähnlicher Form in anderen Prüfungsverfahren vorgelegt.

Copyright Statement

I, Zottl Yves, BSc, hereby declare that this thesis is my own original work and, to the best of my knowledge and belief, it does not:

- Breach copyright or other intellectual property rights of a third party.
- Contain material previously published or written by a third party, except where this is appropriately cited through full and accurate referencing.
- Contain material which to a substantial extent has been accepted for the qualification of any other degree or diploma of a university or other institution of higher learning.
- Contain substantial portions of third party copyright material, including but not limited to charts, diagrams, graphs, photographs or maps, or in instances where it does, I have obtained permission to use such material and allow it to be made accessible worldwide via the Internet.

Signature: _____

Vienna, Austria, June 2024 Zottl Yves, BSc

Acknowledgment

I am thanking Associate Prof. Dipl.-Ing. Dr.techn. Hametner Christoph to make this thesis possible at all and the entire institute of Mechanics and Mechatronics where the investigation took place. During my studies I got the opportunity to learn a lot about control technology. I attended courses and wrote with the help of Professor Hametner a project work about an inverse pendulum wheel. During the preparation of this thesis I was well supported by Dott.mag. Dr.techn. Ferrara Alessandro, who helped me with many answers on the data and MATLAB.

Besides the university I was always supported by my family and friends, who encouraged me to bring this thesis to an end. That is why I am grateful to have these people around me and that they were there for me.

Contents

List of Tables

List of Figures

Chapter 1

Introduction

This chapter gives a brief overview of why the focus of development is moving away from combustion engines in today's society. Possible other vehicle power sources can be used, such as electric and fuel cell power. The central part of this thesis is mainly the combination of those two power sources inside a truck. This led to the motivation to implement cooling strategies for the batteries to increase efficiency due to battery degradation in higher temperatures. The third section describes the previously examined studies on various topics, which led to this work today.

1.1 Historical Development

The evolution of the automotive industry has a long history, and various drive technologies have been explored to increase its efficiency until it reaches its current state. Besides all expectations, electrically powered cars are among the first developments in this field. It is hard to pinpoint the first invention of the car, but in the 1800s, the first electric-powered vehicle got on the road. However, who invented the first electric vehicle is still disputed today. The only version tested earlier were steam-powered vehicles. This type of car was not practicable because it required long start-up times and was limited in range. On the other hand, an electric-powered vehicle is easy to drive and has no issues with steam or gasoline. That is why they were very popular with urban residents. The following invention of the four-stroke engine pushed the steam-powered version more and more into the background. Due to difficulties in energy storage, the development of electric cars has also yet to be able to compete with fossil fuels. Gasoline-powered cars were cheaper than the electric version, and the discovery of numerous oil fields lowered gasoline prices. Therefore, the evolution of gasoline-powered cars was preferred, and the electric-powered options were neglected. At the end of the 20th century, environmental impact became a more prominent role, and the demand for fuel-efficient cars began to rise [24, 25]. The first steps besides optimizing combustion engines were their combination with an electric drive system. This was the beginning of a new era with hybrid electric-powered vehicles (HEVs). This kind of development was the pioneer for

many car manufacturers to reduce the use of fossil fuels. This led to more profound research on the electric components and, ultimately, battery improvements, such as higher efficiencies and bigger capacities.

In today's society exists already various types of batteries. To get an overview of all these kinds of batteries, it is possible to plot the energy density in Wh/kg versus the power density in W/kg. With the logarithmic axes, comparing the shallow and high-power performances of different devices is feasible. With the help of a Ragone plot, which is presented in Figure 1.1 it can be seen that the Lithium-ion batteries provide the highest specific power and energy. This is the reason why these types of batteries are mostly used. While the y-axis represents the available energy, the x-axis shows how quickly the energy can be delivered [2].

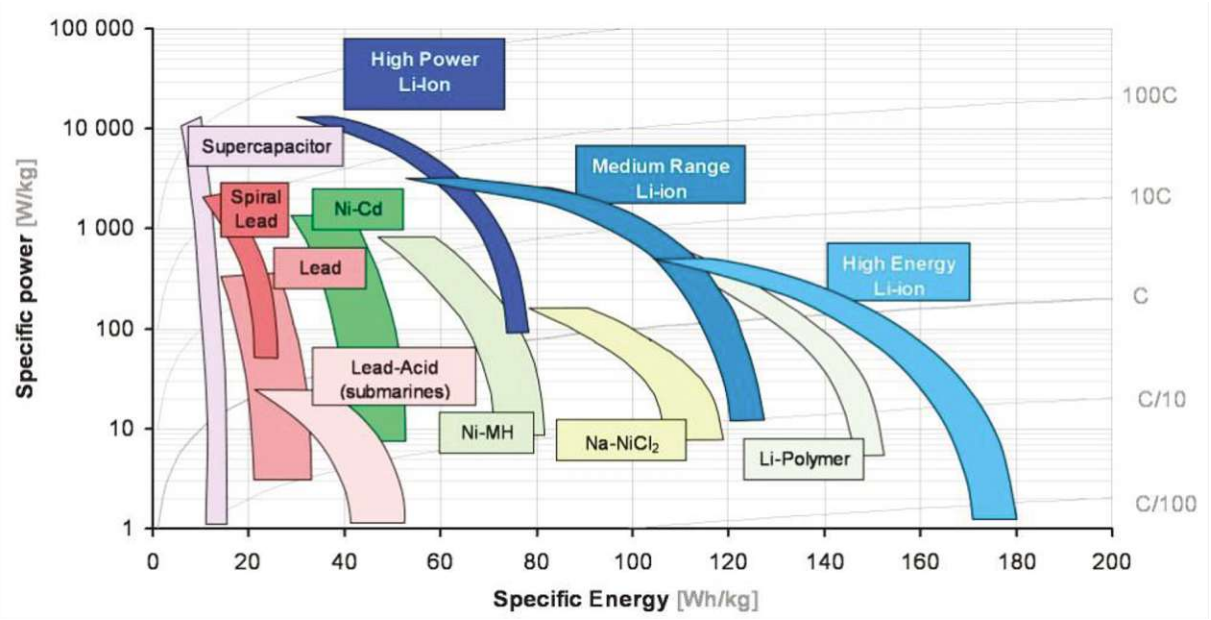

Figure 1.1: Ragone plot for different types of battery cell chemistry [2]

This development of batteries continues to this day, and research is ongoing to create even better options. Different approaches are examined, such as improving efficiency based on extremum seeking control by Wang et al. [26]. Alternatively, add different additives, such as graphene, to Lithium-ion cells [27].

Unfortunately, using lithium-ion cells also has some disadvantages to the environment. Lithium extraction from ores is very energy-consuming and produces waste residue during purification. In addition to optimizing ore mining [28], the reuse and recycling of these batteries are also considered [29, 30]. Nowadays, HEVs and EVs are primarily focused on private and public transport.

Observation on another propulsion system for vehicles is the use of natural gases in combustion engines. For increased energy density, the gas is compressed or liquefied. Liquefied gases must be stored at about $-160°C$, which presents a significant obstacle in infrastructure [31]. Unfortunately, the use of this type of energy has not yet been accepted by society,

and it is uncertain whether this will ever be the case.

To increase the range of electric vehicles, it is possible to use a fuel cell alongside the battery as an additional energy source. In this case, the battery serves as a reserve source, and the fuel cell supplies the energy required for propulsion. Furthermore, the refueling time is shortened. The disadvantages compared to conventional battery-powered vehicles are the currently higher energy costs and the low availability of hydrogen. Presently, there are only a handful of options for refueling [32]. Therefore, some car manufacturers focus on the development only on EVs [33]. However, fuel cell-powered trucks are suitable for long-distance transport, which is why it is discussed in this thesis. Some truck manufacturers have already begun to deliver the first fuel cell-powered vehicles, like Scania [34] or Nikola [35].

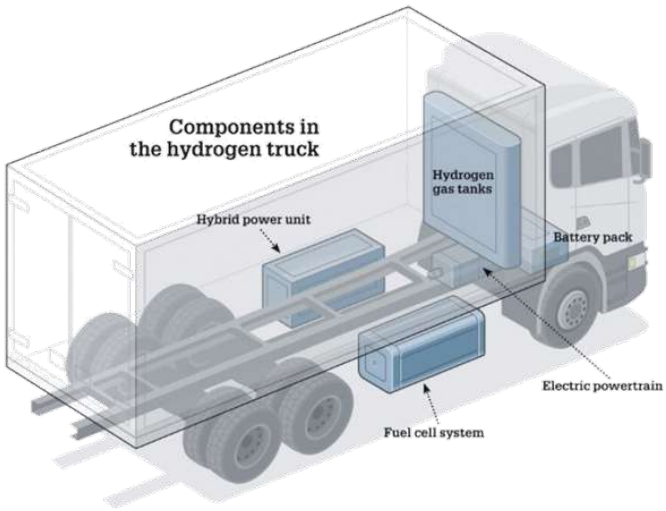

Figure 1.2: Main powertrain components of a fuel cell truck [3]

To give an overview of how a fuel cell truck is built up, schematics of it with its components can be seen in Figure 1.2. The main components are the fuel cell system, which is powered by the hydrogen gas tanks; a battery pack as a backup power source if the fuel cell system can not keep up with the power demand; and a control unit, the hybrid power unit, is added to combine the fuel cell system with the battery pack. This controls the load distribution between these two power sources. The electric powertrain converts this electrical energy from the battery and the DC/DC converter, powered by the fuel cell, into mechanical energy and powers the truck. The power split inside the fuel cell truck and the simplified power flow can be seen in Figure 1.3. Further essential components not shown in these figures are a cooling unit for the fuel cell and the battery pack, where the cooling of the battery pack is complex and will be discussed in greater detail in this thesis.

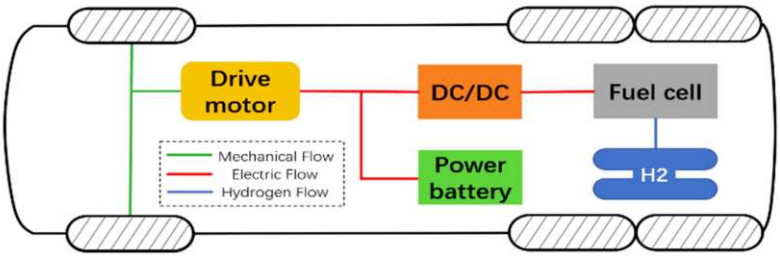

Figure 1.3: Power configuration diagram of a fuel cell truck [4]

1.2 Motivation

A challenging part of the configuration inside a fuel cell truck is the cooling of the components. These include the fuel cells, which operate at the highest temperature level, the battery pack classified as mid-level, then the electric motors as the low level. Each has different operating temperatures where they operate at the highest efficiency. Too high temperatures can lead to the degradation of these parts due to accelerating the chemical reaction and aging process, which decreases life expectancy. As mentioned in the previous section, Lithium-ion batteries are the preferred energy source for electric-powered vehicles. An example of the expected degradation on Lithium-ion cells is illustrated in Figure 1.4. The most dominant degradation mechanism includes the solid-electrolyte interfaces (SEIs) and electronic contact loss through particle cracking. Through high temperatures, the solid-electrolyte interfaces (SEIs) are affected by intensified side reactions, which lead to irreversible capacity loss by consuming active lithium ions [36]. Further, if the battery temperature exceeds a certain point, it can result in a thermal runaway (Figure 1.5). This causes smoke, fire and, in the worst case, an explosion of the cell.

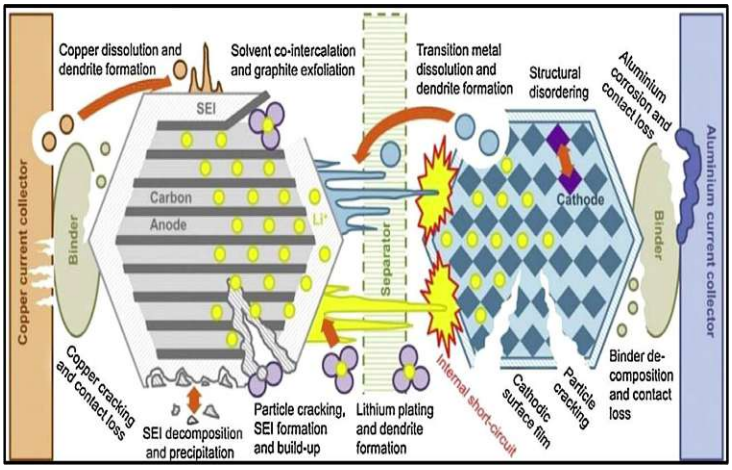

Figure 1.4: Li-ion cell heat generation results [5]

The focus of this thesis is on the thermal management of the battery consisting of Li-ion cells. Its optimal temperature range for this truck battery temperature is between 30 and

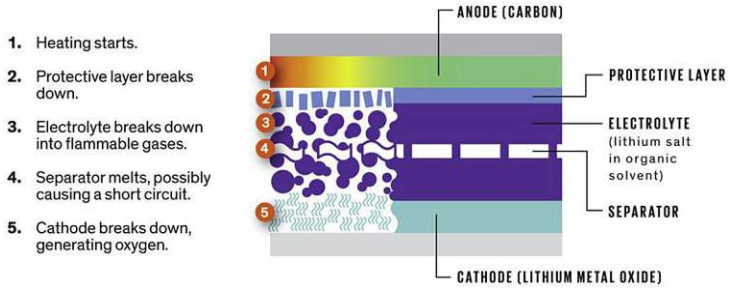

Figure 1.5: Illustration of a thermal runaway process in Lithium-ion battery cells [6]

$45°C$. For this, a cooling strategy has to be developed and examined to prevent overheating of the battery. Typically, vehicles are equipped with radiators for cooling the batteries. Nevertheless, as mentioned before, there is little space, so it can not keep up with the rising temperatures. A more powerful cooling system is a chiller, which also takes up much space inside the truck. Due to limited space inside the fuel cell truck, a standard cooling circuit is not strong enough to dissipate all the produced heat by the battery. Therefore, a suitable solution is to use drive cycles to predict the possible ohmic losses through the battery and counteract with the predictive controller, in this case, a model predictive controller (MPC). With the help of that controller and predictive information, it allows for a predictive cooling of the battery. With this information, the input sequence can be optimized using different weightings. This varies the speed and aggressiveness of the controller. Also, the length of the viewing horizon can be adjusted.

The schematic function of a model predictive controller can be seen in Figure 1.6. A forecast of future signals are required that represents as the prediction horizon. If it did not have this information, it would end up as a typically used hysteresis controller in this situation. This type of controller does not use a horizon to predict future cooling input. This means it sees the current state of the battery temperature and reacts accordingly. It could be sufficient if the cooling circuit is big enough to decrease the temperature in this system. That is the main disadvantage of a hysteresis controller for the cooling circuit of the current fuel cell truck that it would react too late to counter the rising battery temperature. Usually, this would be the standard approach because it does not need a route profile with various amounts of data, just the current and last state of the temperature.

As can be seen in Figure 1.6, the x-axis shows the measurement steps, where k is the current time. The prediction horizon ends at k+p steps and is divided by the sampling time. The goal is that the measured output approaches the reference trajectory. The y-axis represents the output and the required control input. Left from the y-axis is the previous measurement and control input. Additionally to the prediction horizon exists a control horizon, which is smaller than the predictive horizon and represents the computed future inputs. This method uses a cost-minimizing control strategy based on a plant model's iterative, finite horizon optimization.

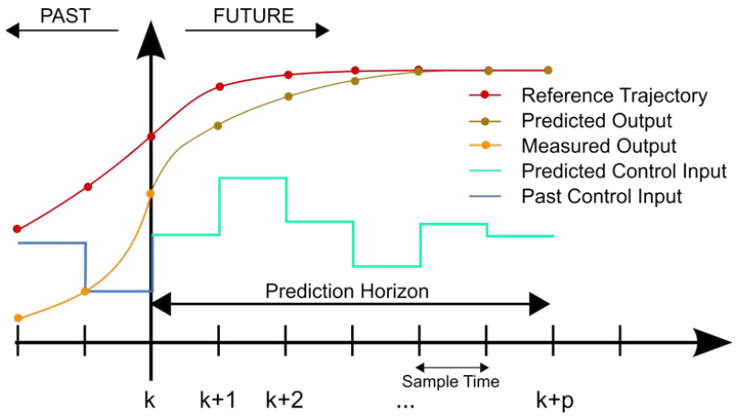

Figure 1.6: Functionality scheme of a MPC [7]

1.3 State of the Art

The concept of thermal management in vehicles has been around for a long time, and there are different approaches depending on the power systems used. Traditional fossil fuel-powered cars typically have a thermostat, a water pump and a radiator fan. This configuration was successfully applied over decades without modification [37].

As batteries began to be used as a power source, whether in a hybrid state or as the primary power source, thermal management gained more attention. This source produces more heat, which has to be kept in a smaller temperature range to increase efficiency. In our daily lives, widely employed battery technology is based on lithium-ion for its superior characteristics of high specific energy and power and long cycling life, as mentioned before [10]. These type of batteries works best in specific temperature range, see Figure 1.7. Due to degradation at higher temperatures, which eventually leads to the destruction of the battery cells, it has to be cooled down. However, the efficiency also decreases when the battery gets too cold.

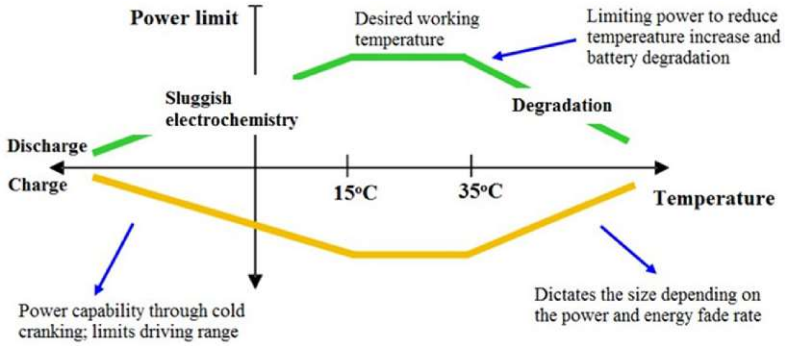

Figure 1.7: Optimal battery operating range [8]

The temperature also affects the internal resistance of the battery, which in turn influences the ohmic losses generated. An overview of four different temperature levels on a Li-ion battery is shown in Figure 1.8, where it can be seen that low battery temperatures raises the internal resistance R_i in $m\Omega$ significantly and increases the ohmic losses of the battery. The

y-axis indicates the state of charge (SOC) for the battery and shows a clear trend downwards to minimum internal resistance around 80 to 90%. Further the temperatures of 30 and 50°C is distinguishable small, which leads to the assumption that the battery has its highest efficiency in that temperature range [9]. That assumption corresponds to the Figure 1.7.

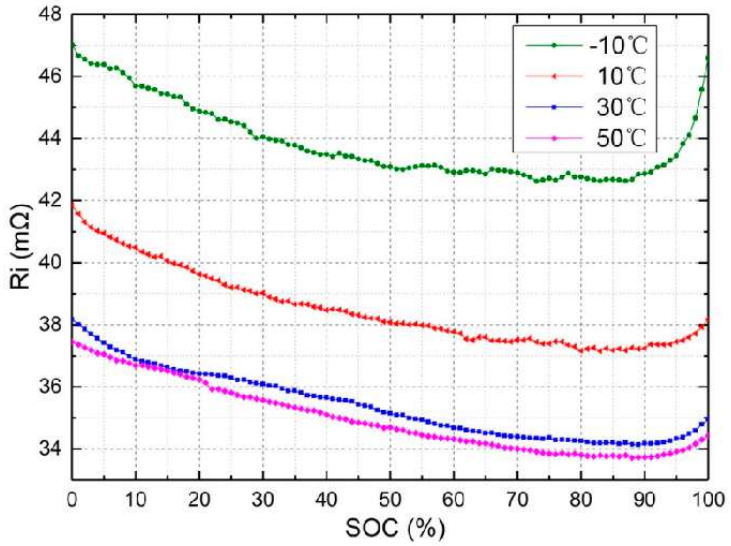

Figure 1.8: Internal resistance of battery over SOC at different temperature levels [9]

The cooling concept also depends on the construction of the battery itself. A for battery thermal management system (BTMS) classification can be seen in Figure 1.9. A good overview of the different cooling concepts and their advantages and disadvantages is given by Lu et al. [38]. The following paragraphs 1.3.1-1.3.3 summarize this topic.

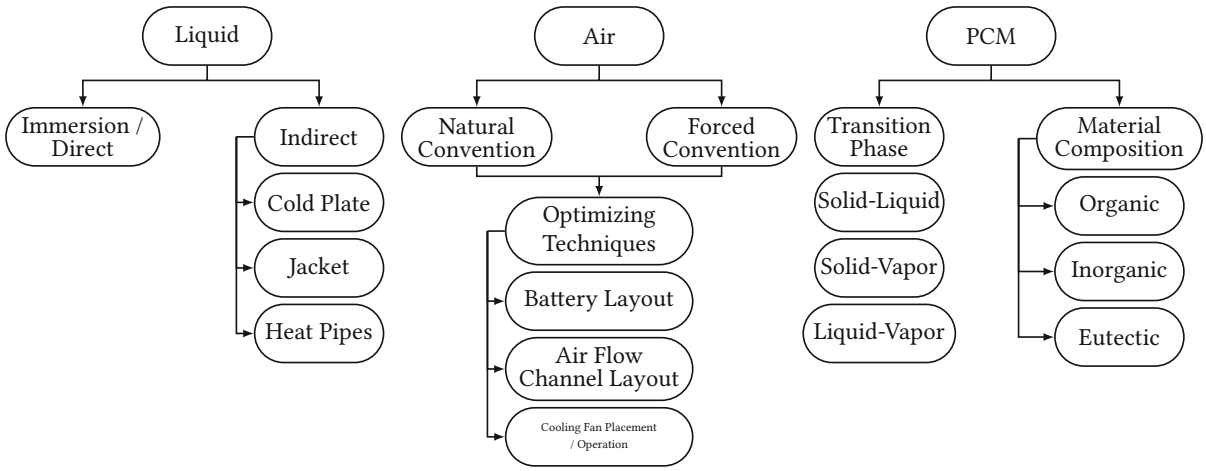

Figure 1.9: Classification of BTMS based on working fluid medium adapted from Liu et al. [10] and Arora [11]

1.3.1 Air Cooling Configuration

The easiest and most traditional approach is the air-cooled configuration, where passive (natural convection) or active (forced convection) cooling is used. A short overview of such structure of Lithium-ion batteries can be seen in Figure 1.10. Here are the cells regularly arranged inside the battery pack, and the air passes through the gaps of these cells. In the case of passive air cooling, the flow of air originates through the relative movement of the vehicle. This means that the cooling may not be sufficient if the car moves too slowly or the ambient temperature is relatively high. A remedy to this problem is installing a fan into the circuit to ensure a minimum airflow for cooling. Additional blowers imply more weight to the vehicle and increase energy consumption. Due to its overall thermal and reliable performance and low manufacturing cost, it is still the main cooling strategy for most original equipment manufacturers (OEMs) [12].

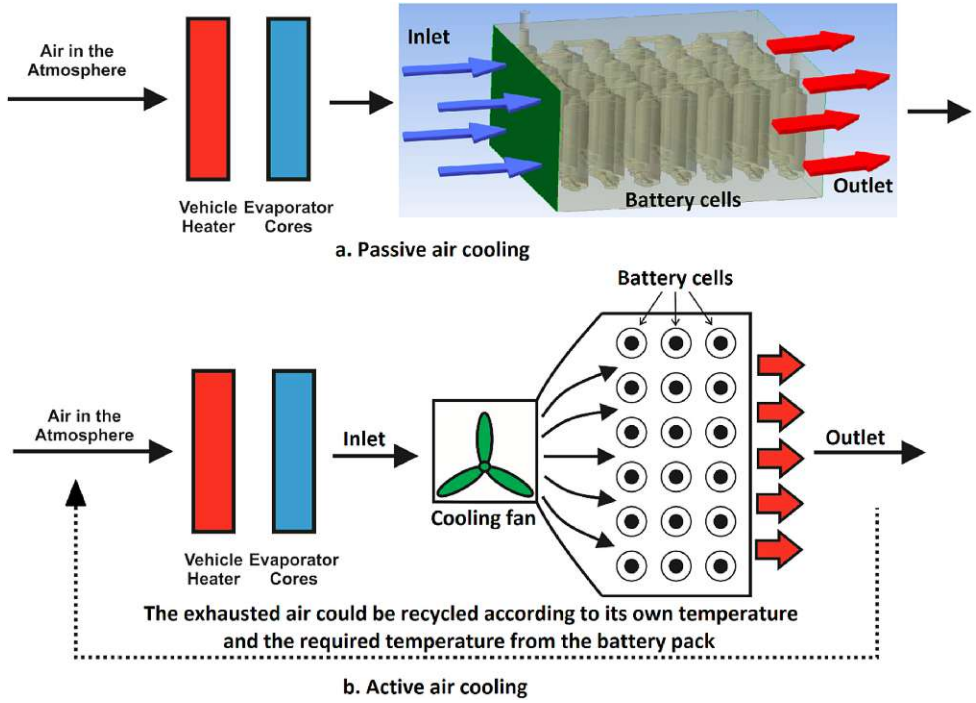

Figure 1.10: Schematic diagram of the air-cooling BTMS [12]

Several improvements for air cooling solutions were researched, and a short overview of these topics is elaborated in the following paragraphs. Among other things, the flow direction through the battery packs was observed by Chen et al. [13]. Variations in the positioning of inlet and outlet vents made it possible to achieve a symmetrical airflow inside the battery packs (Figure 1.11). This and the adopted cell's uneven cell spacing increased the overall cooling performance of the BTMS.

Next to airflow improvements, the arrangement of the cells inside the battery pack was investigated by Fan et al. [39]. Aligned, staggered and cross arrangement were examined,

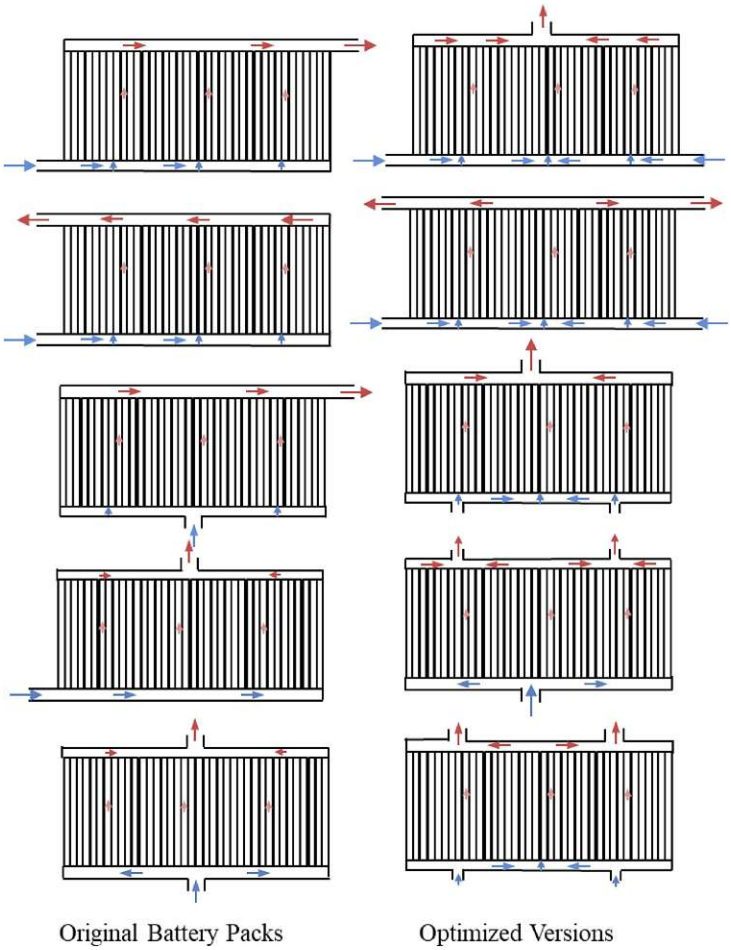

Figure 1.11: Asymmetrical vs symmetrical BTMS battery packs [13]

whereas the aligned setup provided the highest cooling effect. Wang et al. [40] proved an axis-symmetric battery pack layout as the best cooling setup, where the fan sits on top of the cells. The air resistance inside the pack has a big impact on this whole airflow. Tilting the battery pack case about $5°$ reduced this resistance, improving the heat dissipation [41].

An overview of how cell size matters is given by Erb et al. [42]. It is described that the optimization for battery packs depends on specific parameters, and it is possible to minimize the cooling cost. The early stages of the design process help to cut costs and maximize attainable energy density.

1.3.2 Utilization of Phase Change Material for Cooling

Phase change material (PCM) is another solution to decrease the battery's temperature. Naturally, they have a low thermal conductivity, which leads to a higher heat saturation. Therefore, it cannot operate alone for a long time in higher power batteries, see Figure 1.13(a). It can be divided into four different phase change types: solid-solid, solid-liquid, solid-vapor and liquor-vapor. Developments in this section made it possible to increase the cooling power. Re-

searches with different materials, like porous ones (e.g. metal foam) or nanotubes, were made. One promisingly discovery was made with a copper mesh (CM) that is reinforced with paraffin and expanded graphite composite material by Wu et al. [14] (see Figure 1.12). The copper mesh enhanced the heat dissipation performance and the temperature uniformity. This solved the low thermal conductivity, and copper fins allowed the heat to dissipate into the atmosphere. Many developments in optimization in this field enhanced the cycle stability and thermal management even further. Depending on using different materials [43–45] or coupling heat pipes to the system [46].

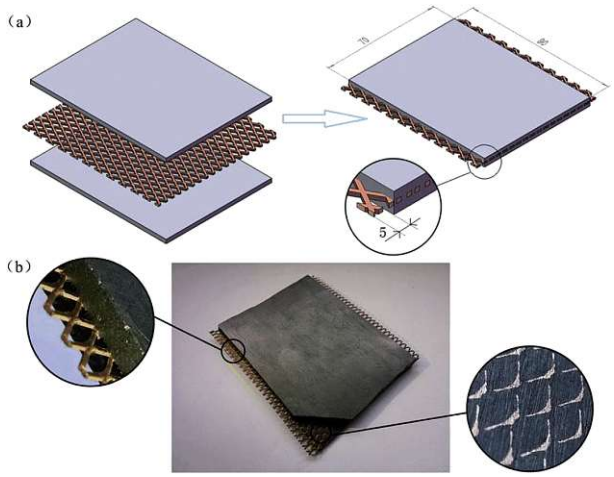

Figure 1.12: (a) Fabrication scheme and (b) Photograph of CM-PCMP [14]

The industry widely prefers heat pipes because it is possible to easily extract the heat of the battery pack outside, where it is easier to be cooled down. This illustration is given in Figure 1.13(b), where fins help dissipate the heat. A fan can be added if the natural convection is insufficient. Figure 1.13(c) shows the heat transfer path of this setup [15].

The heat transfer capability can even be further improved with forced air convection. Fathabadi [47] examined this with the results that it significantly enhanced the cooling power.

An observation of the temperature control of a city bus with a phase exchange material fuel cell (PEMFC) system led to the conclusion that a simple cooling method using normal ON/OFF or PI/PID control is not feasible. This is because of a large time delay of the real system, and therefore, the temperature fluctuations in the phase exchange material fuel cell system can not be easily avoided. Cheng et al. [48] used a first-order Padé method to transform the model into a state-space form with four states. A feedforward controller is used for heat generation at the fuel cell stack and the ambient temperature. A second controller is based on the LQR algorithm as a feedback controller. They achieved good results in the outcome of their observation, where the cooling water temperature is maintained in a range smaller than $\pm 0.5°C$ [48].

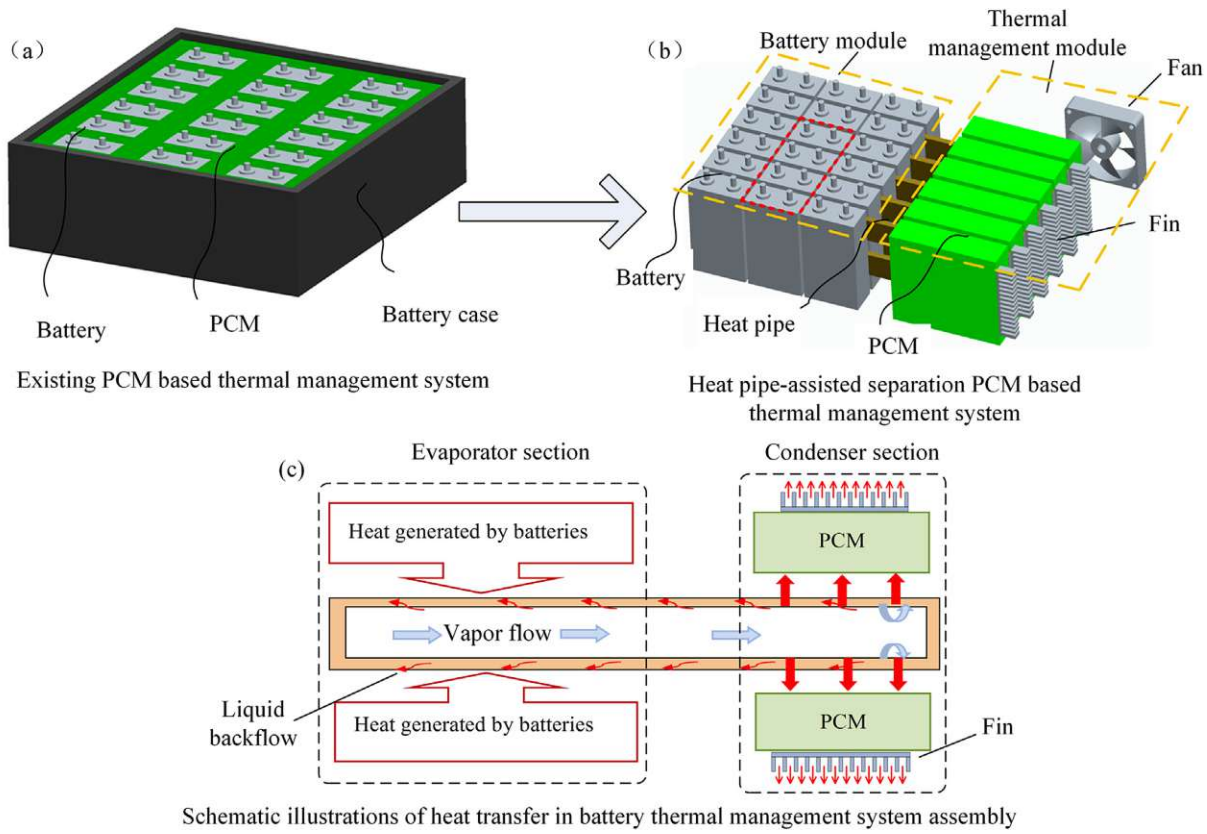

Figure 1.13: Schematic of the battery pack and the seperation type BTMS [15]

1.3.3 Liquid Cooling for Battery Thermal Management

Liquid coolants have a higher heat capacity and conductivity than air cooling. That leads to the highest cooling efficiency and is why it is the most popular solution in electric vehicles [49]. The maximum battery temperature and temperature difference between the battery cells can be reasonably controlled with active regulation of the liquid flow rate. Overall, it depends on the liquid inlet temperature and structural layout inside the battery because higher flow rates inevitably lead to increased pressure drop, decreasing its efficiency [50]. Although it is the most used concept, it has some disadvantages, like a complex layout that includes many components like evaporator, condenser and pumps. All of that increases the weight and cost of the system. The liquid itself poses a threat of causing an electrical short circuit in case of leakage. Therefore, the sealing requirement is essential, and a sealing layer between the liquid and battery is needed, but at the cost of cooling efficiency.

There are different ways to design a liquid cooling setup, like direct contact of the battery with the fluid. In Figure 1.14a, a possible design can be seen with its flow direction. Using different flow pattern designs Figure 1.14b affects the thermal distribution inside the module [51].

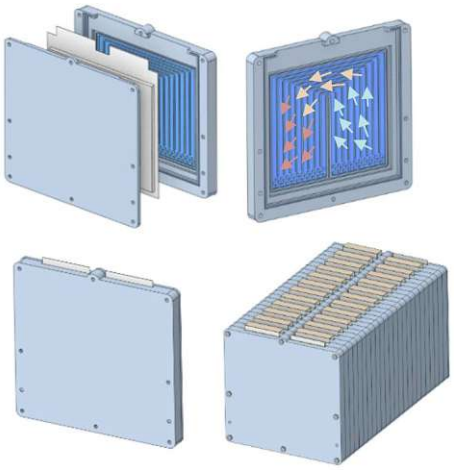

(a) structural design [52]

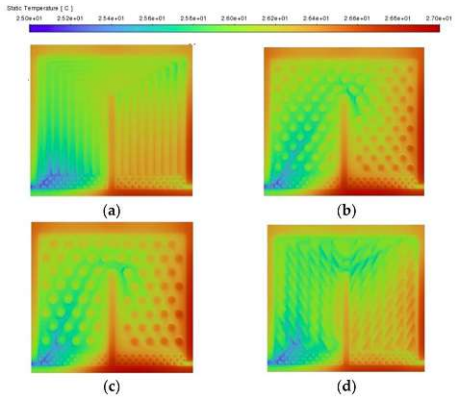

(b) thermal distribution [51]

Figure 1.14: Direct contact liquid cooling with flow pattern of battery cell and module

The design and quantity of channels have a big impact on cooling performance. Ding et al. [53] conclude that a square cooling channel lowers the highest temperature more efficiently. It is also relevant to temperature distribution, the flow rate and direction inside these channels [54, 55].

Cao et al. [56] studied the thermal management of batteries with liquid cooling and PCMs and concluded that the specific latent heat plays a more critical role than thermal conductivity. While Amalesh et al. [57] do not recommend PCMs in hybrid cooling if there is a design constraint on coolant flow rate. Increasing PCMs latent heat leads to no significant improvement in the system. Three designs were observed, two with dielectric coolant and one with hybrid cooling.

1.3.4 Summary of Cooling Methods

Heat spreaders and air cooling are one of the easier solutions when it comes to cooling methods. Through optimization in channeling the air flow the efficiency can be maximized to a certain point. To increase the efficiency further liquid cooling is used. A liquid has a higher efficiency due to the higher heat capacity of the medium and thus can remove more heat. Best solution for cooling strategies is the combination in different methods, such as heat spreaders with air or liquid cooling or phase change materials with liquid cooling. An overview of the different cooling methods are summarized in the Table 1.1.

1.3.5 Energy Management of Electric Vehicles

For optimization of the power distribution in electric vehicles an energy management system is implemented. This system collects and analyze data and efficiently distribute the energy inside the vehicle accordingly. To this end, energy consumption is recorded in real time and

Cooling Method	Techniques/Materials	Advantages/Applications
Heat spreaders	Highly thermal conductive material (e.g. copper) or heat pipes as heat spreaders	- Simple system - Small parasitic power - Very high thermal conductivity using heat pipes
Air cooling	Separate air flow channels for cooling	- Simple system
Liquid Cooling	Cooling channels embedded in battery packs using antifreeze coolant	- Large cooling capability - Efficient cooling - Potential integration for fuel cell water management - Common in large-scale or automobile PEM fuel cell applications
Phase change material (PCM)	Evaporative utilizing latent heat absorption during phase change	- Simplified system - Elimination of coolant pump

Table 1.1: Potential cooling methods and materials [1]

an action plan is developed to improve performance and energy efficiency by monitoring and controlling the savings targets through the system. This reduces the carbon footprint, costs and energy usage by cutting down unnecessary consumption [58].

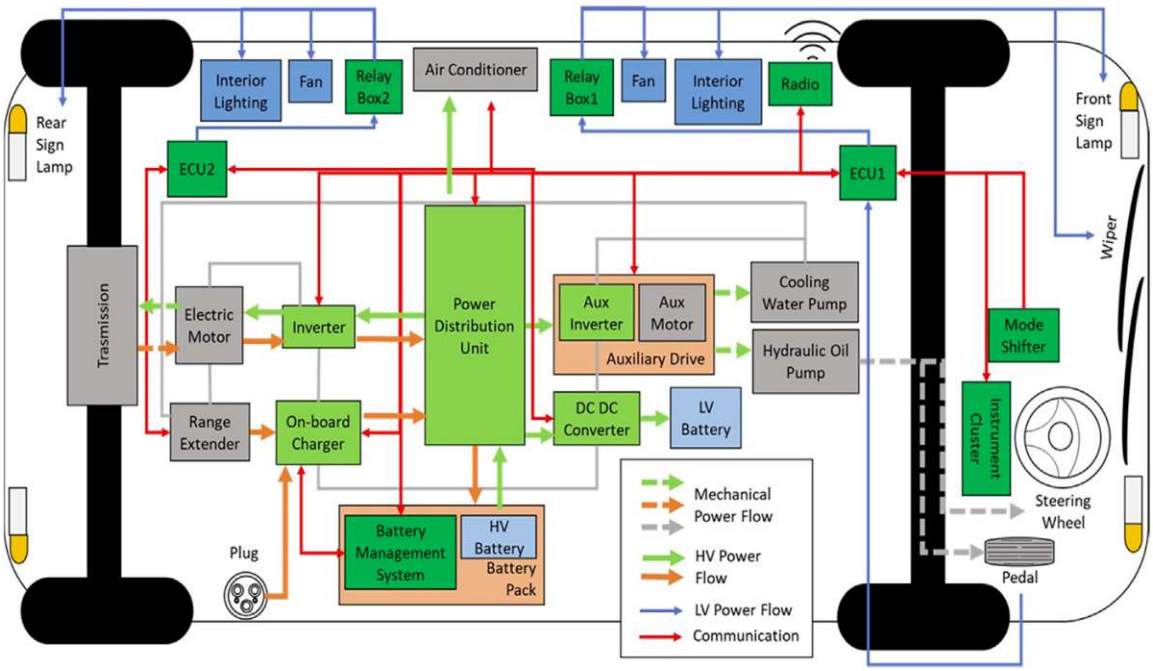

Figure 1.15: Schematic figure of electrical and mechanical power flows in an electric vehicle [19]

In Figure 1.15, the different power flows for the energy management inside an electric

vehicle are displayed, such as the mechanical flow and low and high voltage power flow. The installed power distribution unit manages all of that. Through the transmission, the electric motor propels the wheels as mechanical power. In the case of braking, the power flow can be reversed to regenerate energy into the system. The low-voltage power is connected to a DC-DC converter and provides energy to the auxiliary components, such as fans, lamps, etc. The battery pack consists of the high voltage battery and a battery management system that provides the high voltage power for the electric motor [19].

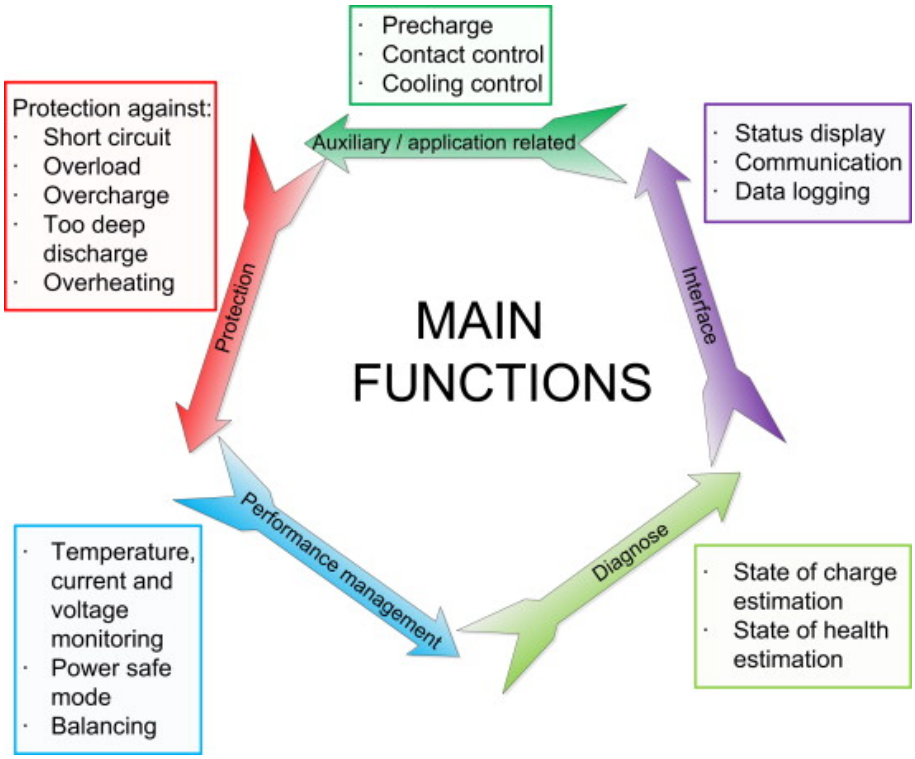

Figure 1.16: Key functions of battery management [16]

A subpart of the energy management is the battery management and it is important for the safe operation of the electrical energy storage systems of electric and hybrid vehicles. In Figure 1.16 the key functions of the battery management is displayed and can be split up in five main functions that all interact with each other. The performance management monitors the temperature, current and voltage and is used for power balancing and a safe power mode. This is diagnosed through the state of charge and state of health estimation. The interface shows the status, logs the data and is applied for communication. It is used for the application that controls the cooling and contact. All is protected against short circuit, overloading as well deep discharge and overheating [16]. In vehicles, several battery cells are connected in series and, or parallel to achieve a bigger capacity. The BMS offers two main topologies for managing power balancing: centralized and master-slave BMS. Both concepts can be seen in Figure 1.17. The centralized BMS is very compact and economical. However, all cells have to be connected directly to the BMS; many wires are needed, making maintenance difficult. For

many battery cells, the master-slave BMS is, therefore, to be preferred. The slave BMS monitors only its designated battery package and controls the charging and discharging process. While the master BMS is the communication point between all the slave BMS and the overall energy management system [17].

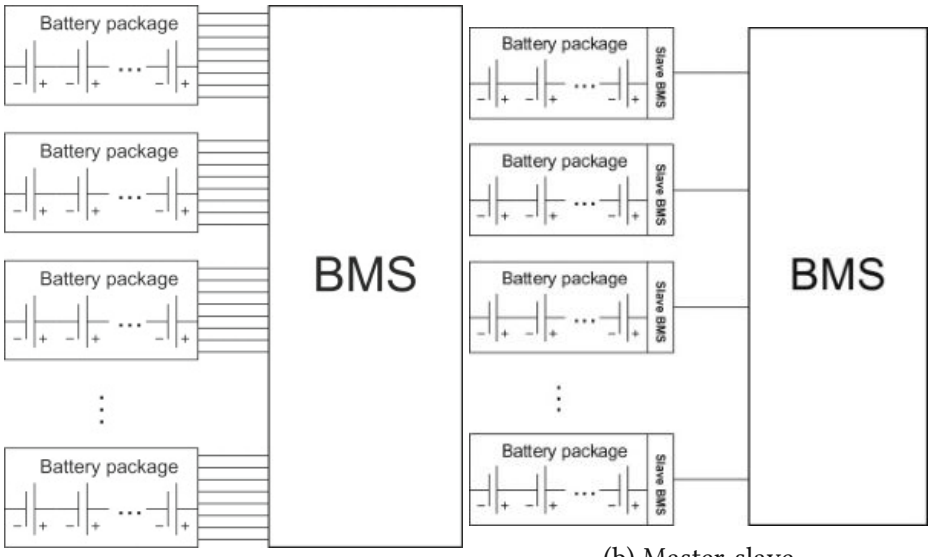

(a) Centralized (b) Master-slave

Figure 1.17: Two different types of BMS [17]

1.3.6 Eco-friendly Transport of the Future

An essential factor for fuel cell vehicles is their affordability in today's society. Like every production scenario, the cost decreases with more produced units. This cost is stated by the value of euro per kilowatt over the annual number of units and can be seen in Figure 1.18. While the material costs decrease with higher units, the manufacturing cost stays relatively constant at the beginning, it slightly increases with higher units. The manufacturing and material cost sums up to the production cost and from that the list price is calculated.

Research about hydrogen-powered fuel cell trucks (HFCTs) has increased almost exponentially over the last few years (Figure 1.19), and many countries are involved in this to lead the transportation sector to a carbon-free future [21]. Progress in optimization is a significant factor in increasing the lucrativeness in this field. Increasing the maximum travel distance while minimizing the cost is essential to push this to an affordable sector for transportation [59]. Aminudin et al. [60] estimate that hydrogen fuel cells will soon significantly affect the transportation industry. The production of fuel cells in large numbers and commercial selling will soon be cheaper, which correlates with Figure 1.18.

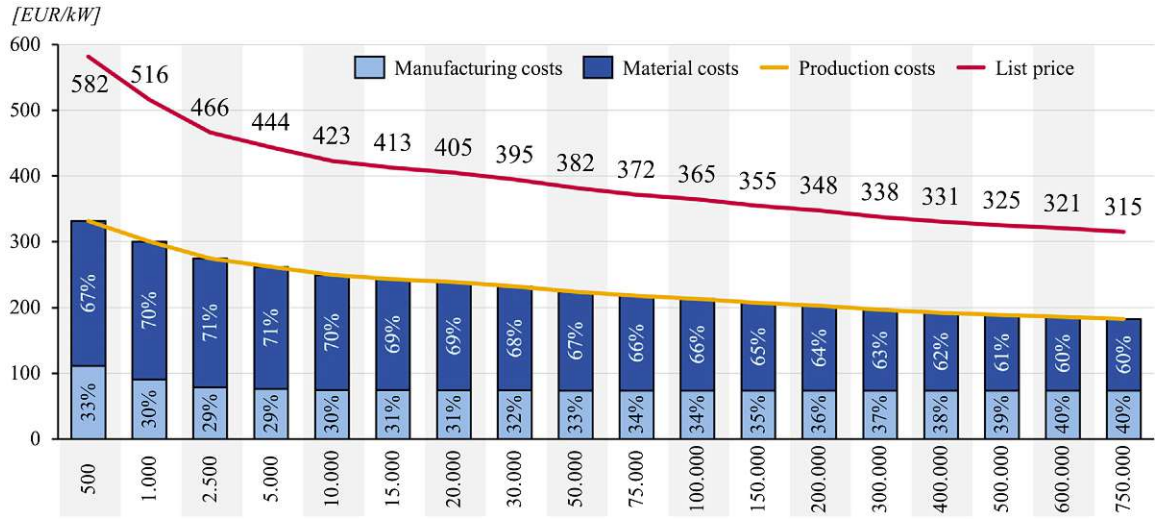

Figure 1.18: Costs of fuel cell systems depending on the annual number of units producedy [20]

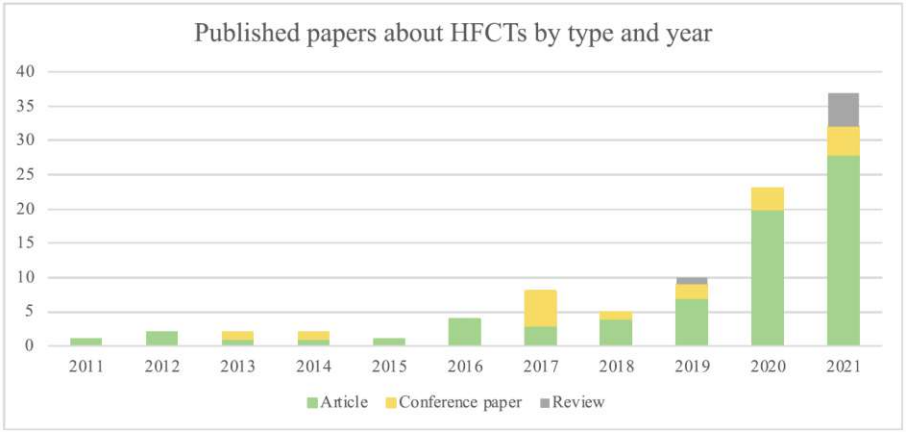

Figure 1.19: Published papers about HFCTs in the last ten years [21]

1.4 Outline of this thesis

One of the main challenging parts for a fuel cell truck is the cooling system due to the three temperature levels: the lower level for electric motors, the mid level for the battery, and the high level of the fuel cell. The battery's temperature must be kept low even during heavy-duty loads. Therefore, this thesis investigates a predictive thermal management system limited to the battery. The reason that it has to be a predictive cooling strategy lies inside the fuel cell truck, where the space is limited. It is impossible to use a regular cooling strategy, such as a simple hysteresis controller, to keep the battery below a specific value, as seen in the next chapter. This work is structured as follows.

Chapter 2 examines the cooling strategy for the battery and how to counter the ohmic losses that accrue when the fuel cell can not compete with the power demand of the required driving force. That usually occurs on steep parts during the route. The battery's cooling circuit is displayed, and the equations for describing the system are derived from this. In order to

verify the equations for the simulation, real driving cycles of conventional diesel trucks were used and prepared for use in the fuel cell truck. These data include the elevation profile, the velocity, and demanding electrical power. In contrast, the electrical power consists of the fuel cell power and the battery. From this electrical battery power, the ohmic losses are derived. In order to use this data for predictive thermal management, it has to be prepared, such as optimizing the computation time. For that the data was resampled to a higher sampling rate due to the necessity for the prediction and control horizon of the model predictive control (MPC) without any loss in information on it.

Chapter 3 uses these prepared driving cycles, and after formulating the mathematical notation for the model predictive control, the system was implemented into MATLAB. The aim was to find an optimal solution in terms of achieving the desired result in keeping the battery's temperature trajectory relatively constant. Additionally, it has to be usable during real-life applications on the fuel cell truck, such as fast computation time during driving to react to deviations from the predefined route profile. Another improvement in the computational time besides the resampling of the driving cycle was achieved for the prediction of the maximum provided cooling power $Q_{chill_{max}}$. The three weighting matrices needed for the MPC were then determined for the input variable, the cooling power, the output variable, the battery's temperature, and the battery's output constraints. Lastly, the prediction and control horizon were examined to increase the efficiency in computational power without losing accuracy during simulation. With the obtained parameters, the thermal model predictive controller was complete, and driving cycles can now be observed. Finally, examples of robustness on the model were investigated, such as deviations form the route profile.

The outcome of this thesis about the investigation for the predictive battery thermal management system inside heavy-duty fuel cell electric truck is summarized in a short conclusion in Chapter 4.

Chapter 2

Battery Thermal Management System

In this chapter, the thermal management system for the battery will be introduced and it will be investigated how the power distribution impacts the temperature of the components. The fundamental mathematical notation for the temperature derived from thermodynamics is described. This information shows the first example of a drive cycle with its contained information. Then, it is explained what kind of preparation has to be done with these drive cycles to implement it for the simulation model. For increased performance in computation time, the data is resampled to a higher sampling rate.

2.1 Cooling Strategy

In the fuel cell truck, there are several thermal systems integrated, one for the fuel cell and one for the battery. In this work, only the thermal management of the battery was described in greater detail. Besides the vehicle's power distribution, the cooling regulation also impacts energy management. While providing power from the battery to the powertrain, the battery begins to heat up. To prevent too high temperatures, a cooling system is implemented. The schematic of the cooling circuit can be seen in Figure 2.1 with the heat transfer displayed in it. On the right-hand side, the battery pack can be found. It is connected to the oil circuit via cooling plates, where the heat loss $\dot{Q}_{loss}$ is transferred. A pump is installed to keep the circuit running. To remove the heat from the system, a chiller is added with its coolant circuit, which is shown in cyan. The coolant circuit consists of the components condenser, evaporator, and compressor. This cooling power of the system is called $\dot{Q}_{chill}$.

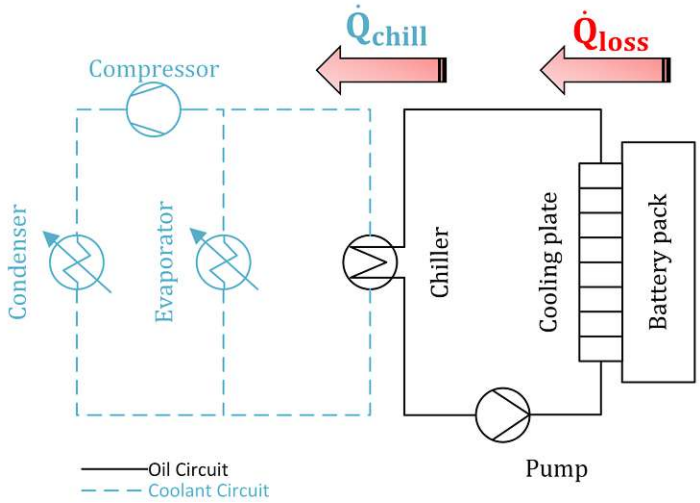

Figure 2.1: Cooling circuit of the battery

The equations can be set up from this cooling circuit for a closed system using the first law of thermodynamics for a closed system. The resulting equations lead to

$$C_{bat}\frac{dT_{bat}}{dt} = \dot{Q}_{loss} - k_1(T_{bat} - T_{oil}) \tag{2.1}$$

$$C_{oil}\frac{dT_{oil}}{dt} = k_1(T_{bat} - T_{oil}) - k_2(T_{oil} - T_{cool}) \tag{2.2}$$

$$C_{cool}\frac{dT_{cool}}{dt} = k_2(T_{oil} - T_{cool}) - \dot{Q}_{chill}(T_{cool}, \dot{m}_{cool}, p_{low}) \tag{2.3}$$

Equation 2.1 describes the temporal change of the temperature multiplied by the heat capacity, which represents the inner energy of the battery. The right side equals the sum of the heat transfer in the system. In this case, the battery's heat loss $\dot{Q}_{loss}$ minus the heat transfer between the battery and the oil circuit happens over the cooling plates as seen in Figure 2.1. Here, the battery's heat loss $\dot{Q}_{loss}$ are the ohmic losses from the battery and represent the disturbance to the system that must be removed.

Next up in Equation 2.2 similar is the inner energy written for the cooling circuit. On the right side is the heat transfer between the battery and cooling circuit and the heat transfer between the oil and coolant circuit. This happens through the chiller in the system.

Lastly, in Equation 2.3 the inner energy for the coolant circuit on the left side and on the right side the heat transfer between coolant and oil circuit minus the chiller power $\dot{Q}_{chill}$. Where $\dot{Q}_{chill}$ is internally dependent on the coolant temperature, mass flow of the coolant, and the pressure in the coolant circuit, this quantity is the controllable source of power that will be delivered to cool the battery's temperature.

The thermodynamic work in this system is neglected, respectively, non existent. The heat transfer between the individual systems as written $k_i dT$, where k_i is a constant factor, depends on the heat exchanger's surface and was provided with these equations for this thesis.

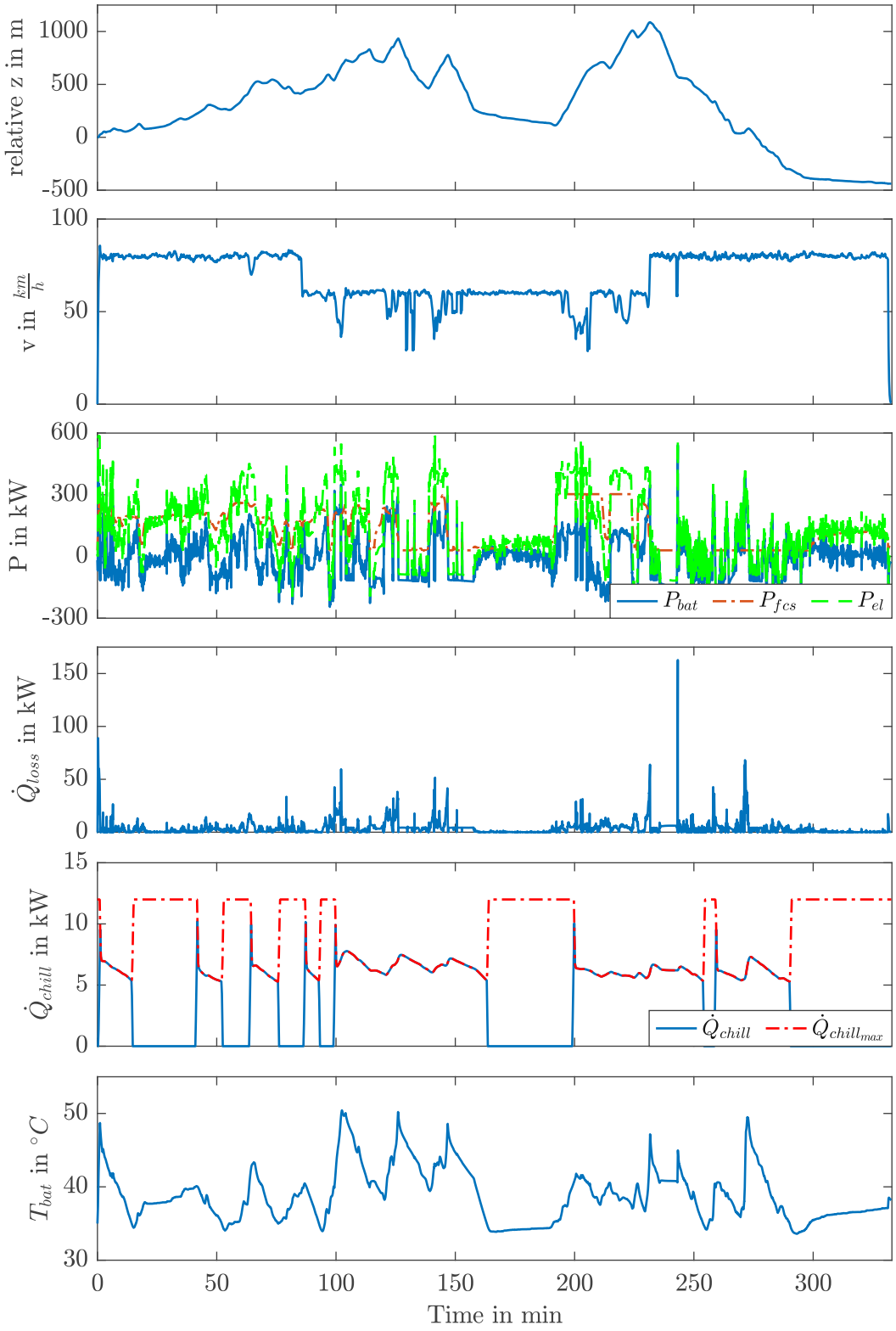

Figure 2.2: Example of a driving cycle

In order to study the mathematical notation and simulation real driving cycles from conventional Diesel trucks are used in this thesis. One example is shown in Figure 2.2.

At the top is the elevation profile, where the vehicle must travel over several inclines and

declines. Right below the estimated velocity can be seen with an averaging speed of $80\frac{km}{h}$ and $60\frac{km}{h}$ in the middle part. These two factors directly impact the power demand on the system, as seen in the third plot. The fuel cell power P_{fcs} quickly reaches its maximum value on the incline part, which leads to the use of the battery power P_{bat}. It can be seen that energy is recuperated back into the battery on the declining route profile. Both powers combined sum up to the electric power train P_{el}. The power split is done by the energy management system of the truck. $\dot{Q}_{loss}$ displays the ohmic losses of the route, which derivatives from the battery power P_{bat}. A hysteresis controller was implemented to calculate the temperature of the battery T_{bat} at the bottom of the plot. Here, the chiller power $\dot{Q}_{chill}$ inhabits only two states, on and off, with a maximum cooling power of about $12kW$. This maximum value was set as a constraint on the controller due to the physical limitations of the fuel truck. As seen, the cooling power can not maintain the maximum value due to efficiency loss.

2.2 Correlation between Predictive EMS and BTMS

Load demand on the fuel cell truck originates from different factors, including current speed and slope. To reduce the complexity of the model, as seen in Figure 2.1, this thesis focuses only on the two parameters: battery temperature and ohmic losses. The power distribution between the fuel cell and battery pack requires an independent energy management system (EMS). It constantly balances the power for the present load demand and helps to extend the fuel cell lifetime by limiting shutdowns and high-power operations. Ferrara et al. [22, 23] analyzed effective adaptive and model predictive control concepts for energy management systems on a heavy-duty fuel cell electric vehicle. In their analysis, they state the challenging aspect of the power-split of hybrid vehicles, as it encompasses various and divergent objectives, including hydrogen consumption, fuel cell voltage degradation, maximum battery temperature, equivalent battery charge/discharge cycles, and SoC control. Figure 2.3 gives an overview of the control architecture for the predictive energy management system. It uses data from the navigation system and the available route information for optimal generation of predictive SoC and FCS power references. With that, an adaptive energy management strategy uses the on-board power split. The same strategy is later used for the predictive battery thermal management system (BTMS) on the battery cooling system.

To verify the improvements of such an adaptive and predictive energy management system, the results for a specific drive cycle (Figure 2.4a) are presented in Figure 2.4b. On top of the fuel cell power, where the adaptive and predictive EMS yields better-balanced power distribution, and the SoC is nearly kept at the reference line. This directly impacts the battery temperature to prevent it from overheating.

Besides the model predictive control, another method was observed: Pontryagin's Minimum Principle (PMP). Both methods use the minimization of a cost function to find its min-

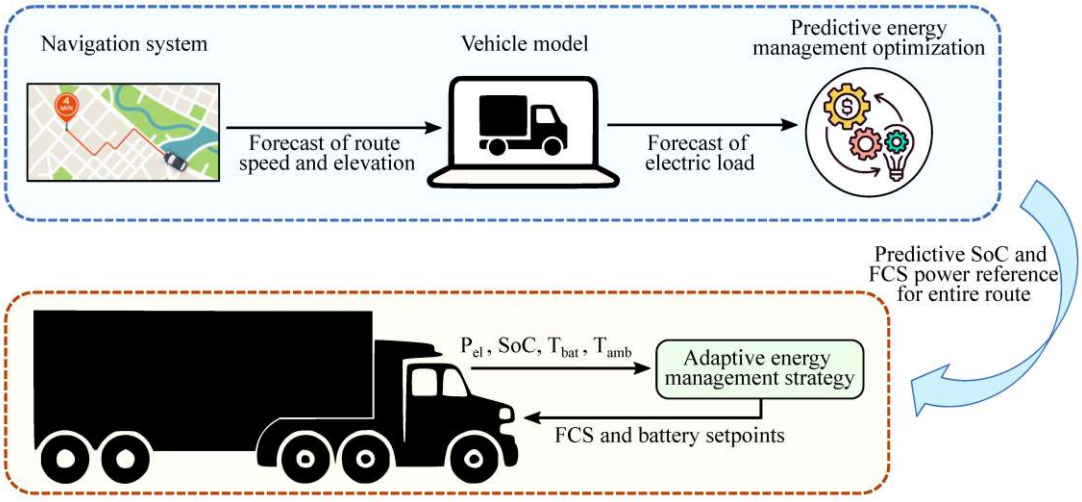

Figure 2.3: Control architecture for predictive energy management system [22]

imum. However, the PMP can not guarantee that it would be the global optimal solution. It requires a complete knowledge of the drive cycle and can only be used offline. Compared to the MPC, which is able to use predicted driving conditions over a finite time horizon and is applicable for online formulation. To implement these control laws, one state variable of the battery state of charge and one control variable as the fuel cell power P_{fcs} was used. The final comparison results between the two control laws, PMP and MPC, can be seen in Figure 2.5. On top is the SOC over time ensuring the battery charge is sustaining for the energy management system. This work resulted in a minimal higher fuel consumption at the MPC method compared to the PMP, but was applicable for online solutions.

The battery's thermal management system reacts directly to the energy management system and counteracts the heat generated. That would be enough if the chiller in that system is strong enough to cool everything down. Therefore, a forecast of the route profile is considered to improve the energy management system, which delivers a prediction of ohmic losses $\dot{Q}_{loss}$. This forecast can then be used for the battery thermal management system to predict the required cooling power. An illustration of this process can be seen in Figure 2.6.

Regarding the information gained through the predictive energy management system, the battery thermal management system can be examined.

2.3 Analysis of the System Model

These prepared drive cycles were now used to verify the implemented MPC. However, it was soon to be seen that the real-time calculation was not feasible. Long prediction and control horizons are required to counteract the undersized cooling concept, which led to an overrun of the actual computing time. Therefore, higher sampling times were examined to reduce the complexity of the discretization. It was possible to use sampling times of up to 60 seconds

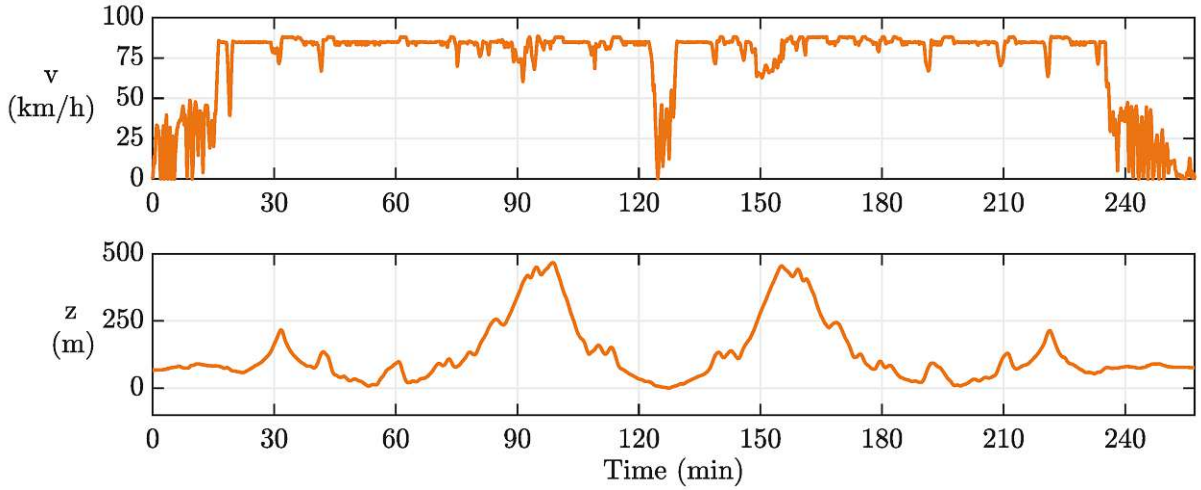

(a) Drive cycle

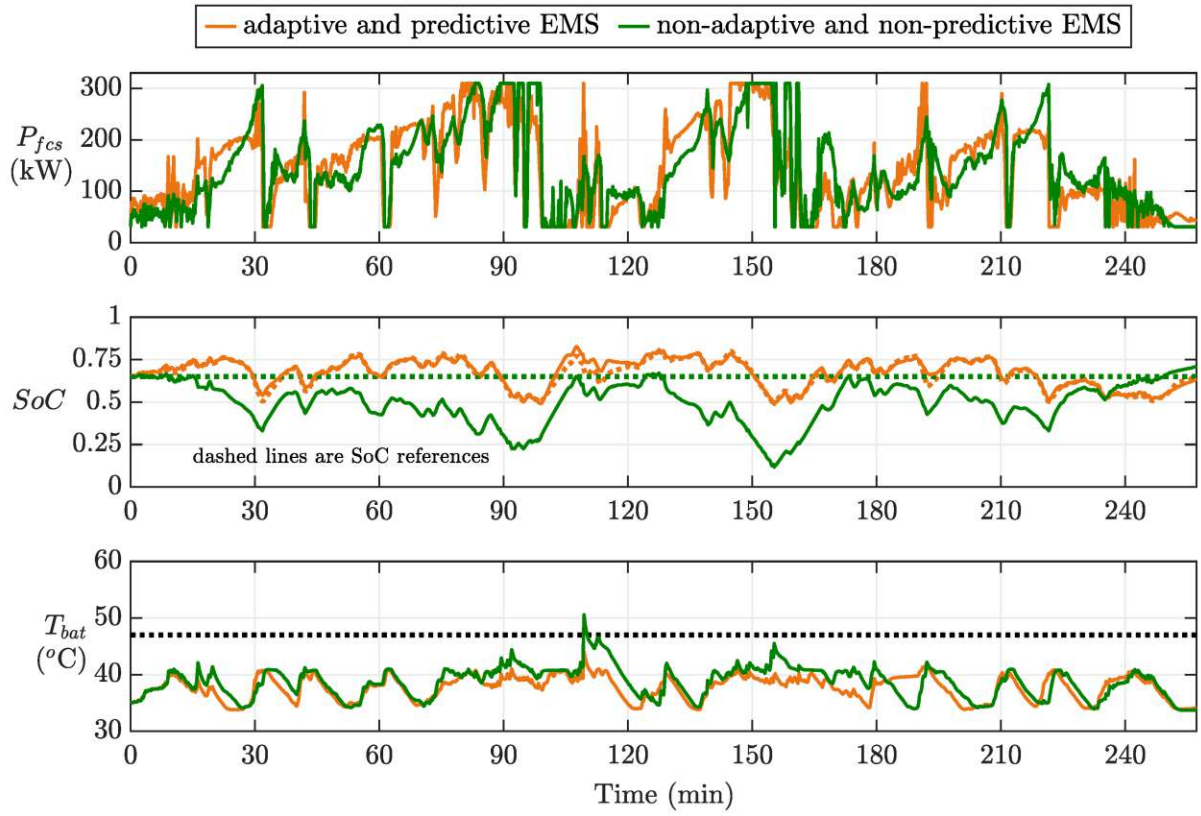

(b) Simulation results at ambient temperature of $20°C$

Figure 2.4: Comparison between predictive and non-predictive EMSs [22]

without negatively impacting the outcome. This can be seen in Figure 2.7 based on a hysteresis controller. In red, the real-time solution is one second compared to a sampling time of 60 seconds in blue. The threshold for the controller lies between 30 and $45°C$, where it turns the chiller on or off.

To recalculate the drive cycles to higher sampling times, using every sampled value was impossible. The heat loss does not just disappear. It had to be summed up for the sampled

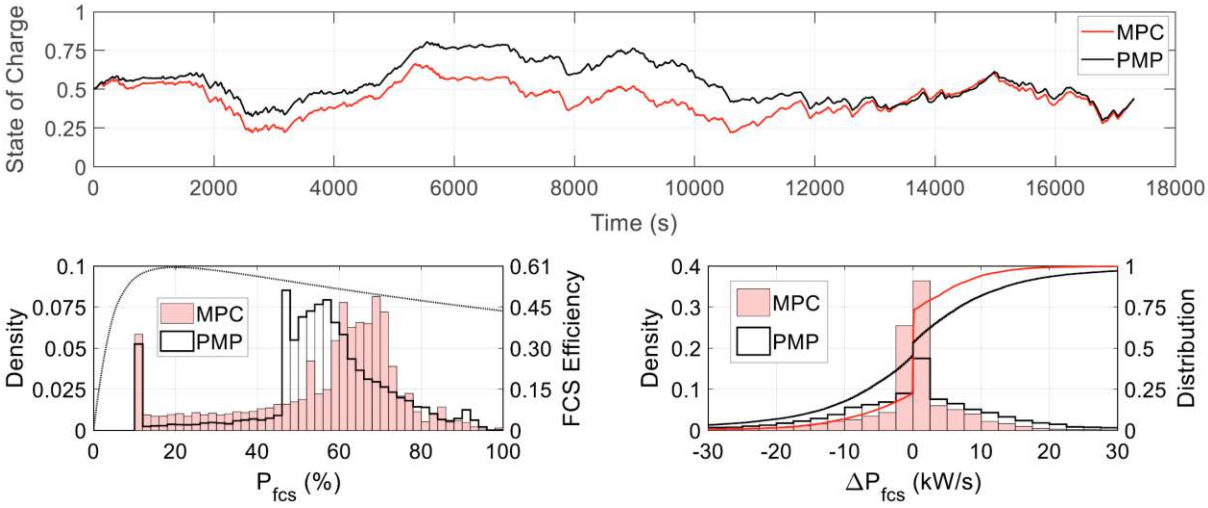

Figure 2.5: Comparison of PMP and MPC (horizon = 10s) results: State of charge (top); FCS operation density (bottom left); FCS power change rate density and distribution (bottom right) [23]

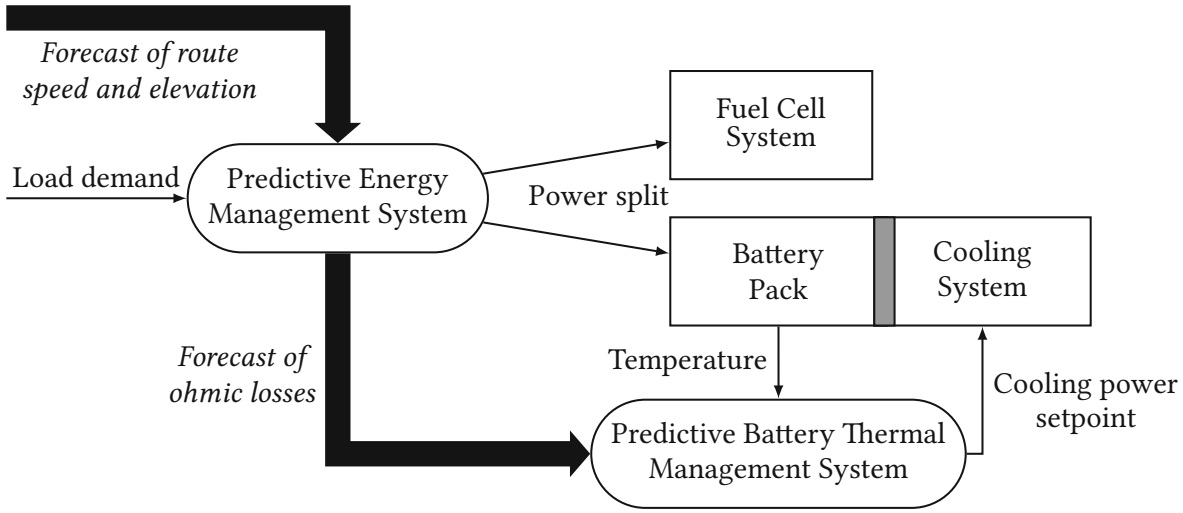

Figure 2.6: Structure of predictive energy and thermal management system

period and compared to the cumulative sum of the real-time data and the data at another sampling time, as shown at the bottom of Figure 2.7. Although the prominent peaks are significantly smaller, the cumulative sum proves they inherit the same energy over the whole horizon.

Summarizing the findings in this chapter, the equations to describe thermal management were stated. With that, it was possible to set up the first optimization, such as increasing the computational speed. That was achieved by resampling the real drive cycles up to 60s while not losing any information. These real drive cycles were derived from conventional Diesel truck routes and adapted for the fuel cell truck.

In the next chapter, the equations will be prepared for the implementation in MATLAB. With the drive cycles from this chapter and the mathematical notation, the simulation can be done. Further investigations into the robustness of the system are observed.

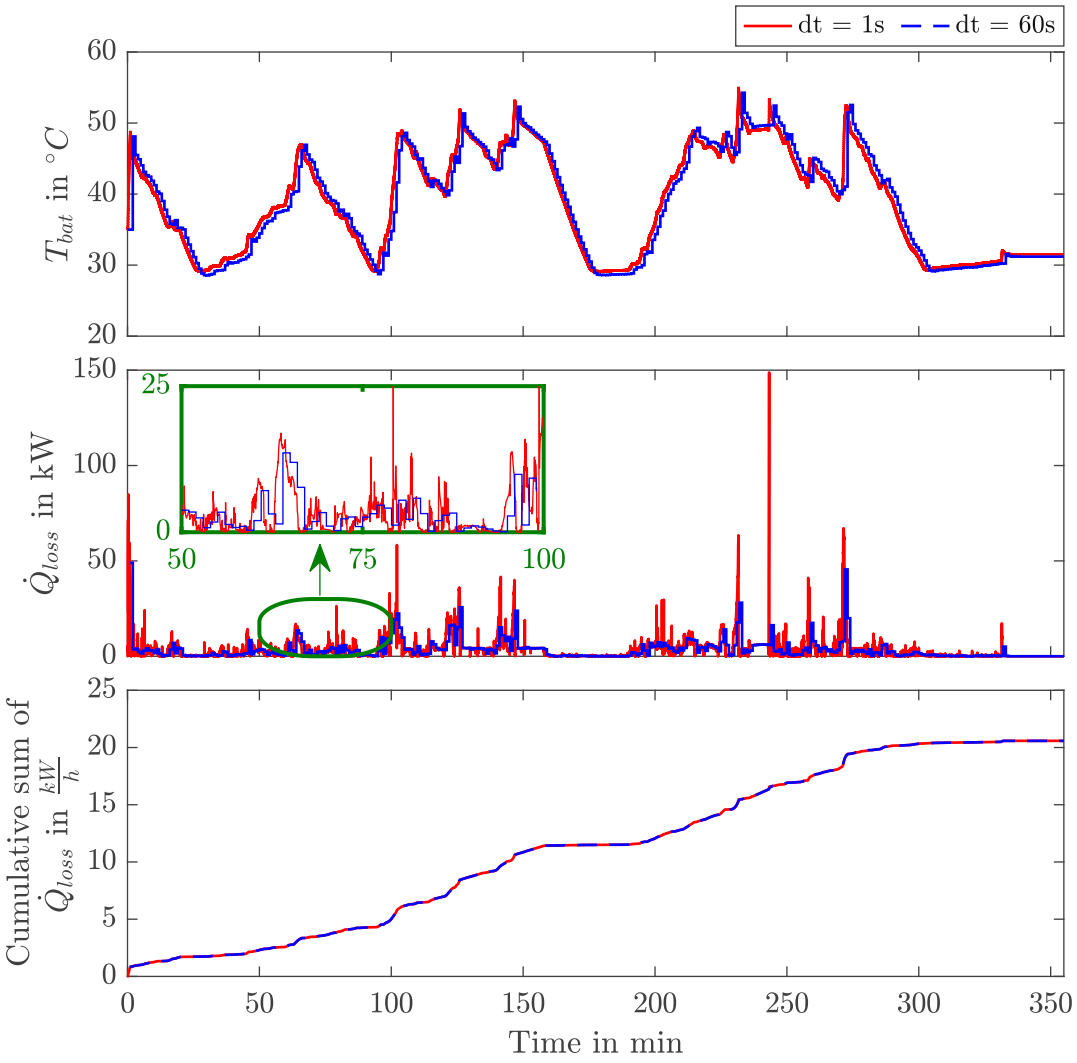

Figure 2.7: $\dot{Q}_{loss}$ and the cumulative sum of a drive cycle for two different sampling times

Chapter 3

Predictive Thermal Management Strategies

This chapter states the mathematical notation for Model Predictive Controller (MPC) and includes a description of these topics. It shows how predictive thermal management can be implemented in a simulation environment. Further, the efficiency in terms of computational time is increased by observing different types of constraints on the maximum chiller power. After that, it was possible to experiment with the weighting matrices and the control and prediction horizons for the MPC to find the optimal solution for the model to achieve the goal of holding the temperature at a certain threshold. Lastly was the investigation of different route profiles on their outcome with the chosen parameters and controlling the robustness of the systems, such as the deviation of the prediction to the actual drive cycle.

3.1 Model Predictive Control

In this thesis, a standard linear model predictive control (MPC) formulation is used to achieve the desired battery temperature through predictive cooling. Model predictive control has a long history and is widely used in the academic community and the industry. While the classical linear quadratic regulator (LQR) operates on a fixed time horizon, which leads to a numerical problem if the prediction horizon gets too large, MPC benefits from a moving time horizon. This offers the possibility for online optimization of a multi-variable control system with soft and hard constraints on the model. Predictive control uses exponential orthonormal functions such as Laguerre and Kautz functions. The mathematical problem can be solved with a continuous time model, which is achieved by a derivative control signal or a discrete-time model by incrementing the control signal [61].

3.2 Mathematical Notation

Proceeding from the model in Figure 2.1 and its resulting Equation 2.1 to 2.3, these are now rewritten into a discrete state space system [61]. Whereas the input vector is stated as the provided cooling power, the disturbance vector is the ohmic losses from the battery. Finally, the desired output vector consists of the temperatures.

$$\boldsymbol{x}_m(k+1) = \boldsymbol{A}_m\boldsymbol{x}_m(k) + \boldsymbol{B}_m u(k) + \boldsymbol{E}_m z(k) \tag{3.1}$$

$$y(k) = \boldsymbol{C}_m\boldsymbol{x}_m \tag{3.2}$$

To do this the equations were divided by the heat capacity for each line. The results can be written directly in matrix notation

$$\underbrace{\begin{bmatrix} T_{bat}(k+1) \\ T_{oil}(k+1) \\ T_{cool}(k+1) \end{bmatrix}}_{\boldsymbol{x}_m(k+1)} = \underbrace{\begin{bmatrix} \frac{-k_1}{C_{bat}} & \frac{k_1}{C_{bat}} & 0 \\ \frac{k_1}{C_{oil}} & \frac{-k_1-k_2}{C_{oil}} & \frac{k_2}{C_{oil}} \\ 0 & \frac{k_2}{C_{cool}} & \frac{-k_2}{C_{cool}} \end{bmatrix}}_{\boldsymbol{A}_m} \underbrace{\begin{bmatrix} T_{bat} \\ T_{oil} \\ T_{cool} \end{bmatrix}}_{\boldsymbol{x}_m(k)} + \underbrace{\begin{bmatrix} 0 \\ 0 \\ -\frac{1}{C_{cool}} \end{bmatrix}}_{\boldsymbol{B}_m} \underbrace{\dot{Q}_{chill}}_{u(k)} + \underbrace{\begin{bmatrix} \frac{1}{C_{bat}} \\ 0 \\ 0 \end{bmatrix}}_{\boldsymbol{E}_m} \underbrace{\dot{Q}_{loss}}_{z(k)} \tag{3.3}$$

The state vector $\boldsymbol{x}_m(k)$ contains the three temperatures from the battery, the oil circuit and the cooling circuit. The input vector $u(k)$ is equal to the cooling power $\dot{Q}_{chill}$ multiplied by its input matrix $\boldsymbol{B}_m$ ($n_x \times n_u$). Lastly, the disturbance vector $z(k)$ refers to the heat loss $\dot{Q}_{loss}$ of the battery. The direct feed through of the input does not exist, as a result, that the matrix $\boldsymbol{D}_m$ is empty and therefore, the equation for the output vector $y(k)$ with its size $n_y \times n_y$ yields to

$$y(k) = \underbrace{\begin{bmatrix} 1 & 0 & 0 \end{bmatrix}}_{\boldsymbol{C}_m} \boldsymbol{x}_m(k) \tag{3.4}$$

This state space formulation must now be augmented to suit a predictive control scheme. A different operation on both sides achieved this. The resulting augmented state space model

$$\overbrace{\begin{bmatrix} \Delta\boldsymbol{x}_m(k+1) \\ y(k+1) \end{bmatrix}}^{\boldsymbol{x}(k+1)} = \overbrace{\begin{bmatrix} \boldsymbol{A}_m & \boldsymbol{0}_m^T \\ \boldsymbol{C}_m\boldsymbol{A}_m & 1 \end{bmatrix}}^{\boldsymbol{A}} \overbrace{\begin{bmatrix} \Delta\boldsymbol{x}_m(k) \\ y(k) \end{bmatrix}}^{\boldsymbol{x}(k)} + \overbrace{\begin{bmatrix} \boldsymbol{B}_m \\ \boldsymbol{C}_m\boldsymbol{B}_m \end{bmatrix}}^{\boldsymbol{B}} \Delta u(k) + \overbrace{\begin{bmatrix} \boldsymbol{E}_m \\ \boldsymbol{C}_m\boldsymbol{E}_m \end{bmatrix}}^{\boldsymbol{E}} \Delta z(k) \tag{3.5}$$

$$y(k) = \underbrace{\begin{bmatrix} \boldsymbol{0}_m & 1 \end{bmatrix}}_{\boldsymbol{C}} \underbrace{\begin{bmatrix} \Delta\boldsymbol{x}_m(k) \\ y(k+1) \end{bmatrix}}_{\boldsymbol{x}(k)} \tag{3.6}$$

Where $\boldsymbol{0}_m$ is a zero matrix with a size of $n_y \times n_x$.

After the state space equations have been set up, the cost function J (Equation 3.7) must be defined. This function must be minimised for optimal results by finding the parameter vector

$\Delta \boldsymbol{U}$. It can be defined with different weighting of inputs and outputs to control the speed and quality of the outcome.

$$J = (\boldsymbol{Y}_{ref} - \boldsymbol{Y})^T \boldsymbol{Q}_y (\boldsymbol{Y}_{ref} - \boldsymbol{Y}) + \boldsymbol{S}^T \boldsymbol{Q}_S \boldsymbol{S} + \Delta \boldsymbol{U}^T \boldsymbol{R}_u \Delta \boldsymbol{U} \tag{3.7}$$

The term Y refers to the battery temperature, which is the central temperature the chiller should control. It can be adjusted with the quadratic output weight $\boldsymbol{Q}_y$ and describes how strong the temperature should be kept close to the reference temperature. The next term is the slack variable or soft constraint quadratic weight $\boldsymbol{Q}_S$ on the system and defines the limits for the temperature. A soft constraint turns into a hard constraint at a high value, and the temperature is kept within the limit. Finally, the impact of the chiller can also be manipulated by the linear weight $\boldsymbol{R}_u$ and can be seen as the speed of the cooling system. A linear weighting of the slack variable was not considered in this progress.

Now we can insert for the term $\boldsymbol{Y} = \boldsymbol{F}\boldsymbol{x}(k) - \boldsymbol{\Phi}_u \Delta \boldsymbol{U} - \boldsymbol{\Phi}_z \Delta \boldsymbol{Z}$ and rearrange the equation that leads to

$$\begin{aligned} J =& (\boldsymbol{Y}_{ref} - \boldsymbol{F}\boldsymbol{x}(k) - \boldsymbol{\Phi}_z \Delta \boldsymbol{Z})^T \boldsymbol{Q}_y (\boldsymbol{Y}_{ref} - \boldsymbol{F}\boldsymbol{x}(k) - \boldsymbol{\Phi}_z \Delta \boldsymbol{Z}) + \dots \\ & - 2\Delta \boldsymbol{U}^T \underbrace{\boldsymbol{\Phi}_u^T \boldsymbol{Q}_y (\boldsymbol{Y}_{ref} - \boldsymbol{F}\boldsymbol{x}(k) - \boldsymbol{\Phi}_z \Delta \boldsymbol{Z})}_{-\boldsymbol{f}_u} + \boldsymbol{S}^T \underbrace{\boldsymbol{Q}_S}_{\boldsymbol{H}_s} \boldsymbol{S} + \Delta \boldsymbol{U}^T \underbrace{(\boldsymbol{\Phi}_u^T \boldsymbol{Q}_y \boldsymbol{\Phi}_u + \boldsymbol{R}_u)}_{\boldsymbol{H}_u} \Delta \boldsymbol{U} \end{aligned} \tag{3.8}$$

The matrix $\boldsymbol{F}$ contains the prediction horizon N_p and has a dimension of $N_p \times n_x$, whereas the n_x equals the augmented row size of $\boldsymbol{B}$. The matrix $\boldsymbol{\Phi}$ has a Toeplitz structure and contains the prediction and control horizon, resulting in a dimension of $N_p \times N_c$. This matrix exists for the input $\Delta \boldsymbol{U}$ as well the disturbance vector $\Delta \boldsymbol{Z}$.

From this equation, we can define elements of an optimization vector $\boldsymbol{f}_u$ and parts of the Hessian matrix $\boldsymbol{H}_s$ and $\boldsymbol{H}_u$. This can be written as

$$\boldsymbol{f} = \begin{bmatrix} \boldsymbol{f}_u \\ \boldsymbol{f}_s \end{bmatrix} \qquad and \qquad \boldsymbol{H} = \begin{bmatrix} \boldsymbol{H}_u & \boldsymbol{O}_s \\ \boldsymbol{O}_s & \boldsymbol{H}_s \end{bmatrix} \tag{3.9}$$

For $\boldsymbol{f}_s$ a zero vector with the same dimension $N_p \times 1$ was implemented due to the consistency of the optimization vector's matrix. The resulting Hessian matrix contains the quadratic weighting for the output and slack variable. A zero matrix $\boldsymbol{O}_s$ with the exact dimensions $N_c \times N_p$ as each submatrix had to be added.

To implement the operating constraints in MATLAB, some equations must be set up. Three expressions are considered: the input rate $\Delta \boldsymbol{U}$, the input $\boldsymbol{U}$ itself and the output $\boldsymbol{Y}$. Auxiliary

matrices $\boldsymbol{M}$ and $\boldsymbol{N}$ are implemented for simplification. The inequality for the input rate is expressed as

$$\Delta \boldsymbol{U}^{min} \leq \Delta \boldsymbol{U} \leq \Delta \boldsymbol{U}^{max} \tag{3.10}$$

Transferring it into matrix form leads to

$$\underbrace{\begin{bmatrix} -\boldsymbol{I} \\ \boldsymbol{I} \end{bmatrix}}_{\boldsymbol{M}_{du}} \Delta \boldsymbol{U} \leq \underbrace{\begin{bmatrix} -\Delta \boldsymbol{U}^{min} \\ \Delta \boldsymbol{U}^{max} \end{bmatrix}}_{\boldsymbol{N}_{du}} \tag{3.11}$$

Whereas the input vector is written

$$\underbrace{\begin{bmatrix} \boldsymbol{u}(k) \\ \boldsymbol{u}(k+1) \\ \vdots \\ \boldsymbol{u}(k+N_c-1) \end{bmatrix}}_{\boldsymbol{U}} = \underbrace{\begin{bmatrix} \boldsymbol{I} \\ \boldsymbol{I} \\ \vdots \\ \boldsymbol{I} \end{bmatrix}}_{\boldsymbol{C}_1} \boldsymbol{u}(k-1) + \underbrace{\begin{bmatrix} \boldsymbol{I} & \boldsymbol{0} & \dots & \boldsymbol{0} \\ \boldsymbol{I} & \boldsymbol{I} & \dots & \boldsymbol{0} \\ \vdots & & \ddots & \\ \boldsymbol{I} & \boldsymbol{I} & \dots & \boldsymbol{I} \end{bmatrix}}_{\boldsymbol{C}_2} \underbrace{\begin{bmatrix} \Delta \boldsymbol{u}(k) \\ \Delta \boldsymbol{u}(k+1) \\ \vdots \\ \Delta \boldsymbol{u}(k+N_c-1) \end{bmatrix}}_{\Delta \boldsymbol{U}} \tag{3.12}$$

Considering the inequality similar to the input rate in Equation 3.10 leads Equation 3.12 to following matrix form

$$\underbrace{\begin{bmatrix} -\boldsymbol{C}_2 \\ \boldsymbol{C}_2 \end{bmatrix}}_{\boldsymbol{M}_u} \Delta \boldsymbol{U} \leq \underbrace{\begin{bmatrix} -\boldsymbol{U}^{min} + \boldsymbol{C}_1 \boldsymbol{u}(k-1) \\ \boldsymbol{U}^{min} - \boldsymbol{C}_1 \boldsymbol{u}(k-1) \end{bmatrix}}_{\boldsymbol{N}_u} \tag{3.13}$$

Lastly the output constraint is stated as

$$-\boldsymbol{S} + \boldsymbol{Y}^{min} \leq \boldsymbol{F}\boldsymbol{x}(k) + \boldsymbol{\Phi}_u \Delta \boldsymbol{U} + \boldsymbol{\Phi}_z \Delta \boldsymbol{Z} \leq \boldsymbol{Y}^{max} + \boldsymbol{S} \tag{3.14}$$

Rewritten in matrix form to conform the previous results leads to

$$\underbrace{\begin{bmatrix} -\boldsymbol{\Phi}_u \\ \boldsymbol{\Phi}_u \end{bmatrix}}_{\boldsymbol{M}_y} \Delta \boldsymbol{U} + \underbrace{\begin{bmatrix} -\boldsymbol{I} \\ -\boldsymbol{I} \end{bmatrix}}_{\boldsymbol{M}_s} \boldsymbol{S} \leq \underbrace{\begin{bmatrix} -\boldsymbol{Y}^{min} + \boldsymbol{F}\boldsymbol{x}(k) + \boldsymbol{\Phi}_z \Delta \boldsymbol{Z} \\ \boldsymbol{Y}^{max} - \boldsymbol{F}\boldsymbol{x}(k) - \boldsymbol{\Phi}_z \Delta \boldsymbol{Z} \end{bmatrix}}_{\boldsymbol{N}_y} \tag{3.15}$$

Combining these equations (3.11, 3.13 and 3.15) with the auxiliary matrices and considering

the slack variables leads to the following equation

$$\underbrace{\begin{bmatrix} \boldsymbol{M}_{du} & \boldsymbol{O}_s \\ \boldsymbol{M}_u & \boldsymbol{O}_s \\ \boldsymbol{M}_y & \boldsymbol{M}_s \end{bmatrix}}_{\boldsymbol{M}} \underbrace{\begin{bmatrix} \Delta \boldsymbol{U} \\ \boldsymbol{S} \end{bmatrix}}_{\boldsymbol{\xi}} \leq \underbrace{\begin{bmatrix} \boldsymbol{N}_{du} \\ \boldsymbol{N}_u \\ \boldsymbol{N}_y \end{bmatrix}}_{\boldsymbol{\gamma}} \tag{3.16}$$

Whereas the matrix $\boldsymbol{M}_s$ ($n_y \cdot N_p \times n_y \cdot N_p$) is an identity matrix specified as above, and the matrix $\boldsymbol{O}_s$ ($N_c \times n_y \cdot N_p$) is empty. These two are needed because of the slack variable $\boldsymbol{S}$ and serve the purpose of implementing constraints to the system.

Most of the derivations in this chapter can be found in *Model Predictive Control System Design and Implementation Using* MATLAB by Wang [61] with some additions such as the slack variables.

Now, formulating the optimization problem is possible with all those equations. Therefore, reformulating Equation 3.8, whereas the first notation can be neglected because this does not influence the optimal solution $\boldsymbol{\xi}^*$. With the variables as stated, gives the following mathematical statement

$$\begin{aligned} \boldsymbol{\xi}^* = \arg \min_{\boldsymbol{\xi}} \quad & \frac{1}{2} \boldsymbol{\xi}^T \boldsymbol{H} \boldsymbol{\xi} + \boldsymbol{f} \boldsymbol{\xi} \\ \text{such that} \quad & \boldsymbol{M} \boldsymbol{\xi} \leq \boldsymbol{\gamma} \end{aligned} \tag{3.17}$$

In the next sections possible constraints are observed for a feasible solution for provided drive cycles. Implementing the constraints with the Equation 3.16 in MATLABleads to the desired initial situation for the simulation.

3.3 Implementation and Simulation

Stating the augmented state space equation (Equation 3.2) and the optimization problem (Equation 3.17), it is now feasible to find an optimal solution. With the MATLAB in-built function *quadprog(**H**,**f**,**M**,**N**)* the constrained optimization problem can be solved.

The implemented cooling circuit is limited in power and can not provide infinite cooling energy. That is the reason why a maximum chiller constraint has to be implemented. This limitation affects the predicting cooling power over the whole prediction and control horizon. The first solution used the maximum power of $10kW$ over the whole prediction horizon, shown in red in Figure 3.1. Due to physical limitations, the chiller cannot provide this constant power because the heat absorption depends on the coolant flow, and therefore, this solution was not very convincing. The logical next step was to use the exact maximum chiller

power, which implies a prediction. To achieve that, the previous forecast of cooling power was implemented in the equation of the built-in function. The initialization was the starting condition of an overall maximum of $10kW$. This achieved far better results on the outcome but increased the computational time tremendously. To counter this calculation time, a third possible solution was examined, and that was to use an underestimated maximum power of $5kW$ over the prediction horizon. The result does not vary much from the predicted version, but the computational time decreased by about 40%. Therefore, the logical step was to use the underestimated approach for the simulation.

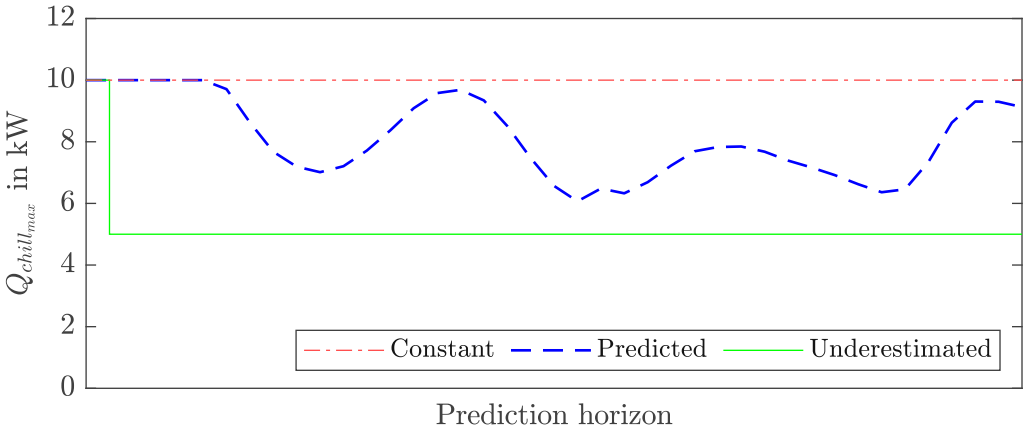

Figure 3.1: Constraints of $Q_{chill_{max}}$

The realization of the real-time solution was achieved using Simulink. Figure 3.2 shows an overview of the structure of the calculation path. Starting at the top, the real-time data is shown in orange that goes directly into the battery cooling system, which is schematically shown in Figure 2.1. The real-time data includes the external influences such as the ambient temperature $T_{ambient}$ and the heat loss $\dot{Q}_{loss}$ that is dissipated by the battery. Additionally, the cooling power $\dot{Q}_{chill}$, which the MPC calculates in red, is another input for the battery cooling system. These outputs the three temperatures T_{bat}, T_{oil}, T_{chill} and the maximum chiller power $\dot{Q}_{chill_{max}}$ that is currently possible. For the MPC to work, prediction is also needed. These are shown in blue and include a forecast of the route profile, which contains the heat loss $\dot{Q}_{loss}$ and ambient temperature $T_{ambient}$. Inside the MPC block, the calculation is done to provide the needed cooling power, and therefore, the circle closes. This block can calculate solutions at a specific sampling data, which is mentioned in section 2.3.

3.4 Optimization for Full Drive Cycle

A pre-evaluation took place before the real-time implementation in Simulink. This was the optimization for the whole drive cycle or the so-called offline solution for the MPC. To achieve this solution, the prediction and control horizon is set to the entire drive cycle period. The sampling time had to be increased within this calculation because the computation time exceeded

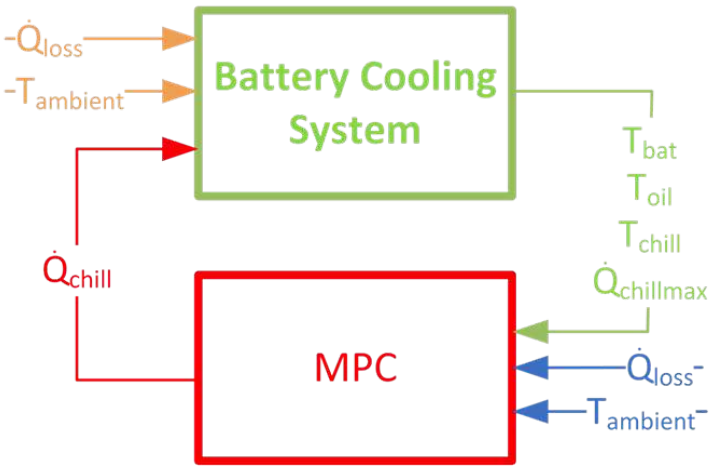

Figure 3.2: Simulink model

real time data — load forecast data from route profile
MPC at specific sampling time — real time simulation at 1s sampling time

the practical benefit. As mentioned in section 2.3, it was possible to go up to 60 seconds for the sampling time without losing the accuracy of the outcome while decreasing the computation time significantly. In order to optimize the full drive cycle, the weighting matrices had to be selected. Therefore, various settings were examined to find the optimal solution. Because the goal was to stay within certain limits for the battery temperature, the weighting $\boldsymbol{Q}_s$ on the slack variable was set very high. The upper boundary is set to $45°C$, and no limit was assumed downward. Conversely, the weighting $\boldsymbol{Q}_y$ on the battery itself did not have to be set high and was kept at the standard value of one. This is because these two variables almost nullify each other when they are set to the same value. In Figure 3.3 (including 3.4), the blue line describes the result for the chosen parameters, which can be found in Table 3.2. A difference in the power distribution of the chiller can be seen in the lower parts of these figures. If both values are very high, the chiller reacts much faster than the settings where both values are set to standard. However, in the end, the outcome of the battery temperature does not differ too much from each other.

The last part of this section was to observe the parameters for the input. The last weighting value **R** was set low to speed up the chiller's reaction. In Figure 3.4, the difference in the speed is visible in the lower subplot. If the R-value is set to one, the system is prolonged and sluggish, trying to avoid the upper boundary. Because of that, the temperature decreases below $20°C$ for that case.

3.5 Online Implementation

The online implementation describes the solution for real-time data and, therefore, during driving. The forecast for this was decreased because the longer the prediction, the less flexible

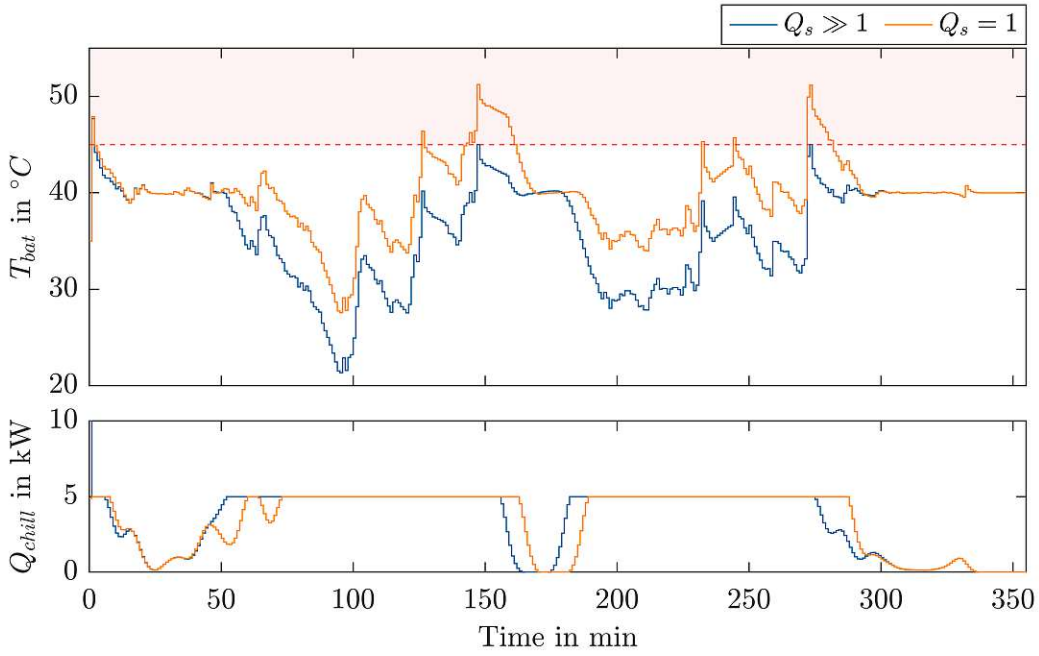

Figure 3.3: Simulation results on different weighting on slack variable

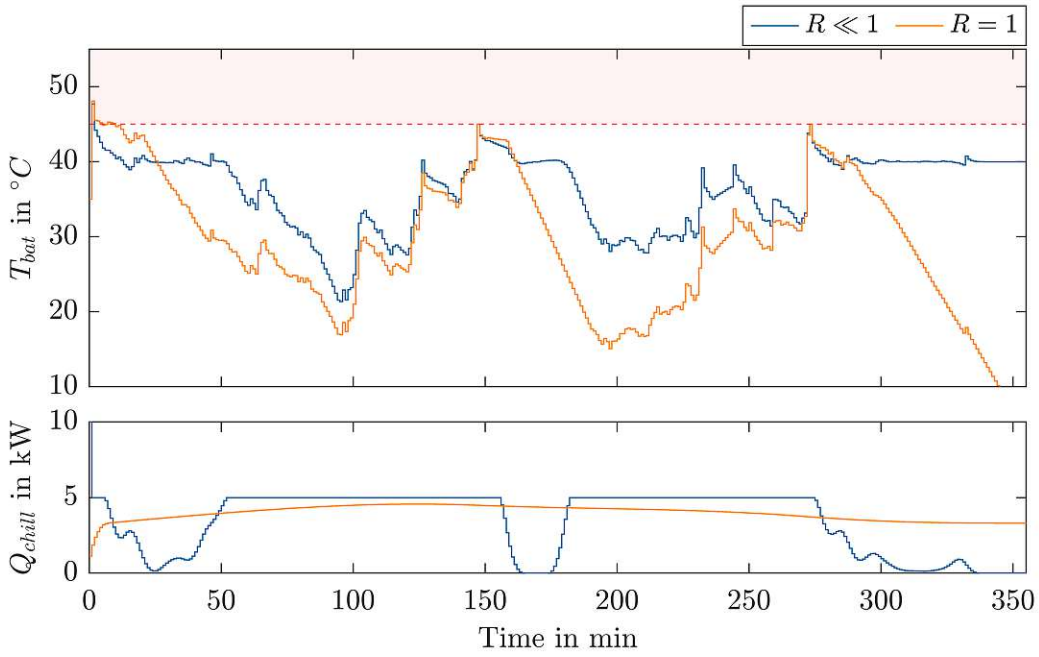

Figure 3.4: Simulation results on different weighting on input

the system can react to unexpected events. The online implementation could be done with information achieved during the full drive cycle optimization. The settings were copied, except for the prediction and control horizon. These were evaluated during this process, and the results can be seen in Figure 3.5 and Table 3.1. In the beginning, both horizons were set equally during the examination. The computation time increased rapidly as the horizon

increased, leading to a slow time constant. In the top sub-figure, the blue line represents a ten-minute horizon length and exceeds the upper $45°C$ temperature mark more often than the other two because the system could not pre-cool the battery fast enough. The calculation is quickly terminated at five seconds, while the green line at 70 minutes horizon length can almost stay below the border. However, the computation time is three times the 40-minute horizon length and can also keep the battery temperature inside the borders. The maximum battery temperature listed in the table for 40 and 70 minutes is equal because of the beginning of the trajectory. Due to the prediction and control horizon length, the MPC cannot correctly process the first peak of the battery heat loss trajectory. Therefore, for comparison, the first five minutes can be neglected to compare the different temperatures for varying prediction horizons, shown in brackets inside the table. The mean battery temperature is also listed in the table and is decreasing by about $1°C$ per 30 minutes. Considering all the information, the best decision was to take the option with the 40-minute horizon length. This combines the accuracy and still fast calculation at the same time .

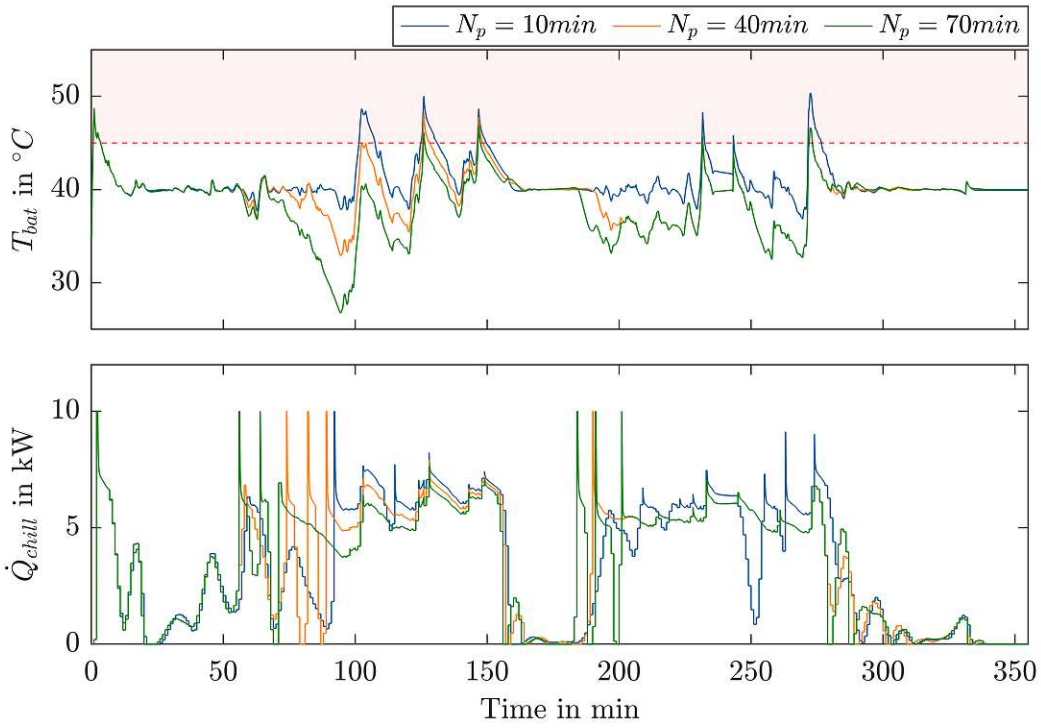

Figure 3.5: Simulation results on different prediction horizons

With the decision on the prediction horizon, the control horizon was observed. Figure 3.6 compares a ten-minute and a 40-minute control horizon. As can be seen, there is not much difference between these two. The calculation time for the shorter one is about seven seconds, which is twice as fast as the one with a control horizon of 40 minutes (see Table 3.1)[1].

[1]These calculation times were achieved with the following pc configuration: Intel i7-4770k @3,9GHz, 12GB DDR3 RAM

Prediction horizon N_p in min	$T_{bat_{mean}}$ in $°C$	$T_{bat_{max}}$ in $°C$	Calculation Time [1] in s
10	40.8 *(40.8)*	50.4 *(50.4)*	5
40	39.5 *(39.4)*	48.7 *(48.0)*	14
70	38.8 *(38.5)*	48.7 *(46.9)*	49

Table 3.1: Difference between prediction horizon and their impact on the calculation *(numbers in brackets neglecting the first 5 minutes of the trajectory)*

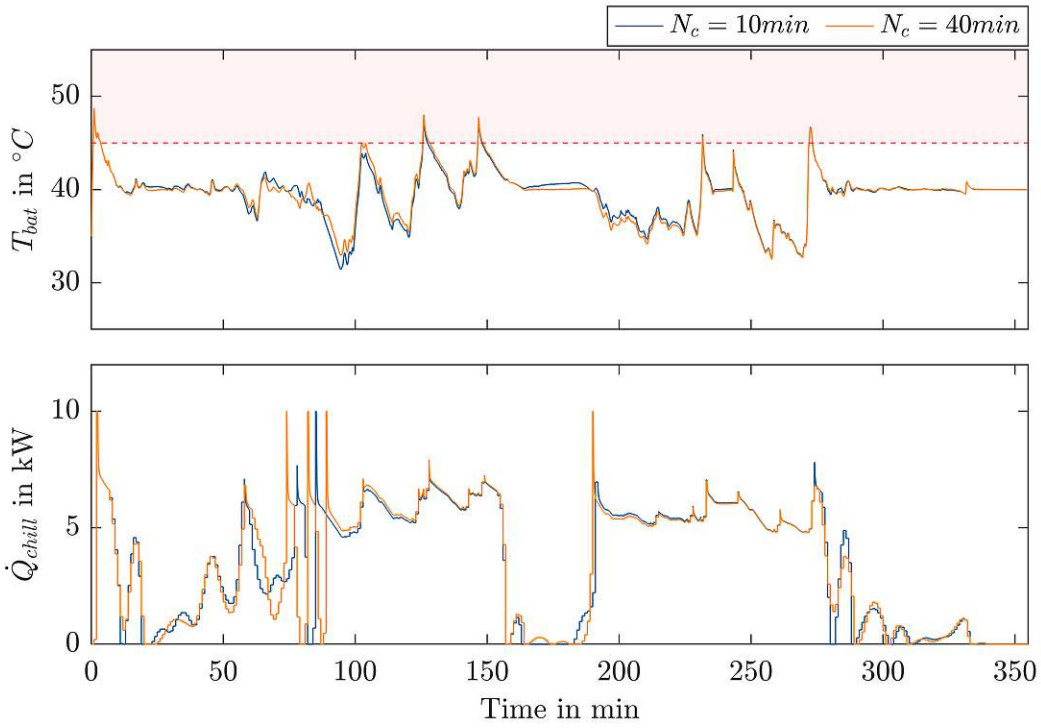

Figure 3.6: Simulation results for different control horizons

Summarizing the observation, the final parameters were chosen for the MPC and can be found in Table 3.2. The resulting trajectory of the battery temperature and the power distribution of the chiller is shown in Figure 3.7. At the top, the battery temperature is plotted in blue, including the upper boundary of $45°C$ and the reference temperature at $40°C$ in red. Due to the limited chiller power, as shown at the bottom, the battery temperature exceeds the upper boundary slightly, but this is neglectable. The heat loss of the battery is visible in the middle part of this figure. The results in numbers for this Figure 3.7 is presented in Table 3.3. These values are already neglecting the first five-minute peak for the heat loss.

sampling Time dt	weighting on output $\boldsymbol{Q}_y$	weighting on input $\boldsymbol{R}$	weighting on slack variable $\boldsymbol{Q}_s$	prediction horizon N_p	control horizon N_c
$60s$	1	$\ll 1$	$\gg 1$	$40min$	$10min$

Table 3.2: Chosen parameters for the MPC

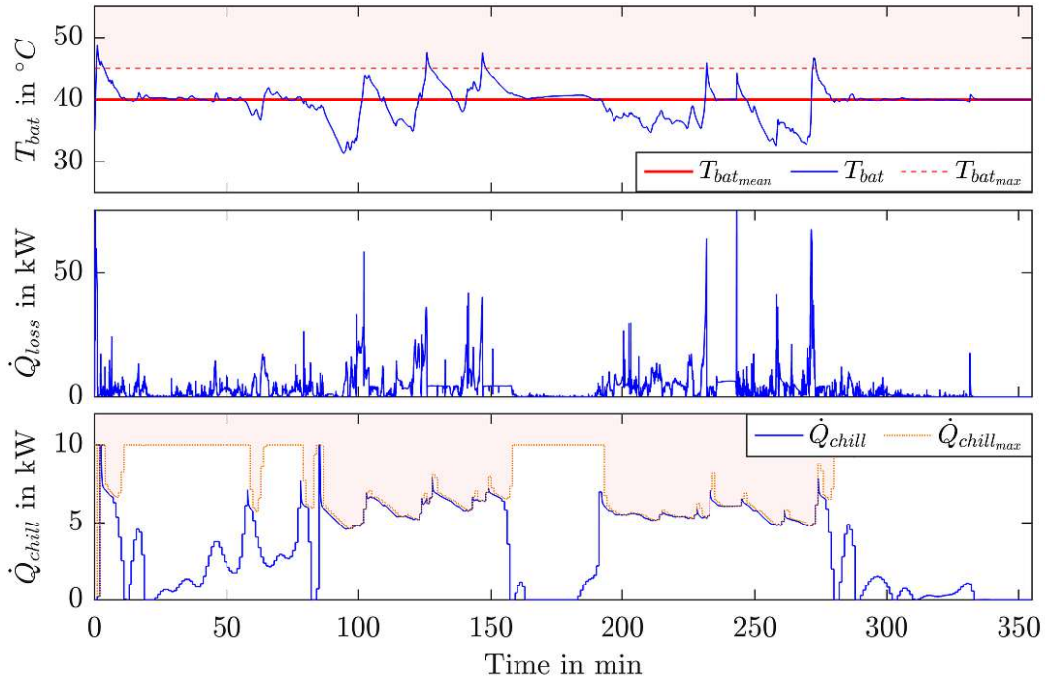

Figure 3.7: Resulting trajectories with chosen parameters

Average heat loss $\dot{Q}_{loss_{mean}}$	Average cooling power $\dot{Q}_{chill_{mean}}$	Average battery temperature $T_{bat_{mean}}$	Maximum battery temperature $T_{bat_{max}}$	Calculation Time t
$3.4kW$	$3.4kW$	$39.4°C$	$47.6°C$	$5s$

Table 3.3: Results for Figure 3.7

3.6 Robustness Investigations

Now that the settings have been defined, the system can be observed for its robustness to various disturbances. These sources of error can occur due to all kinds of unpredicted circumstances due to the fact that the used model is a simplified version from real driving.

Starting with a deviation for the actual heat loss over the predicted heat loss $\dot{Q}_{loss}$, that can result from traffic congestion or not considered construction zones during the route. These lead to a different speed limit, which affects the energy distribution in the system and thus changes the produced heat loss. This is achieved by adding random noise over the data in the range

of $\pm 5kW$. The result of this deviation can be seen in Figure 3.8. Compared to the optimal outcome, which can be seen in Figure 3.7 the resulting temperature rises due to an incorrect prediction. The chiller also works less effectively. As information on different heat loss $\dot{Q}_{loss}$ it has to be mentioned that in Figure 3.8 is displayed summed up for the sampling time of $60s$ compared to the one in Figure 3.7, where it is shown in $1s$ sampling time. The reason for that is a better comparison with the deviation of $\dot{Q}_{loss}$.

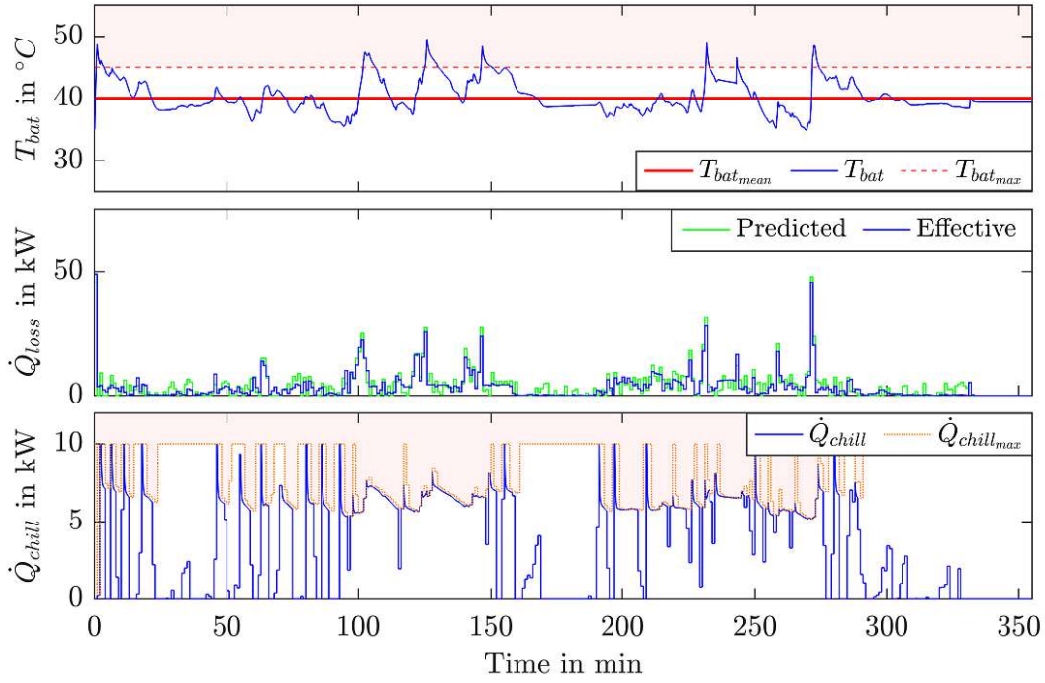

Figure 3.8: Random interference over heat loss $\dot{Q}_{loss}$

Another possible source of error can be a detour due to blocked roads. Then, no data would be available for this forecast and therefore, the predicted heat loss $\dot{Q}_{loss}$ is set to zero for a particular time. An example is shown in Figure 3.9 where no data is available during minutes 200 to 250. As before, when data is incorrect or missing, the temperature on the battery rises because it can not keep up the cooling on site.

Suppose the system receives completely wrong data for the heat loss $\dot{Q}_{loss}$, as shown in Figure 3.10, no reliable outcome can be expected. Such as loading a wrong route profile for the chosen path can lead to this situation. The cooling for the battery is random and will not dampen the temperature peaks of the system.

Another possible interference would be an incorrectly predicted ambient temperature. However, this did not significantly impact the outcome and is therefore not presented in this thesis.

The most likely error in this configuration would be the difference between reality and the model that was used for simulation. This could differ from slightly simplified assumptions to

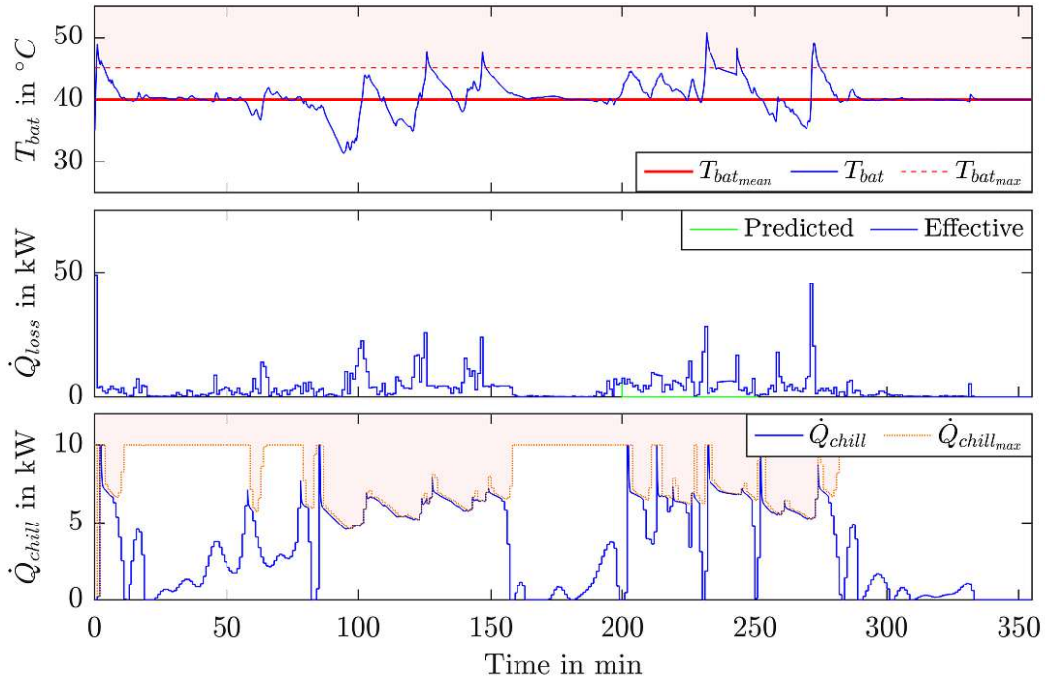

Figure 3.9: Missing data on the prediction for heat loss $\dot{Q}_{loss}$

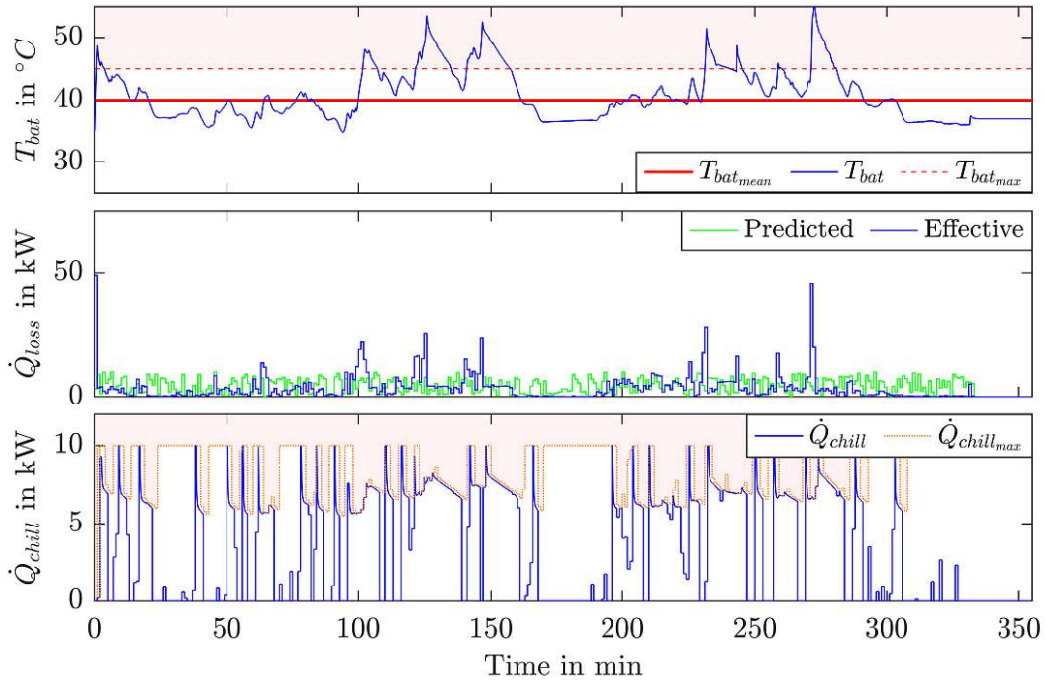

Figure 3.10: Random data for heat loss $\dot{Q}_{loss}$

create the resulting equations for the system model. Another plausible solution is that the internal resistance of each battery deviates from one another with different temperatures and

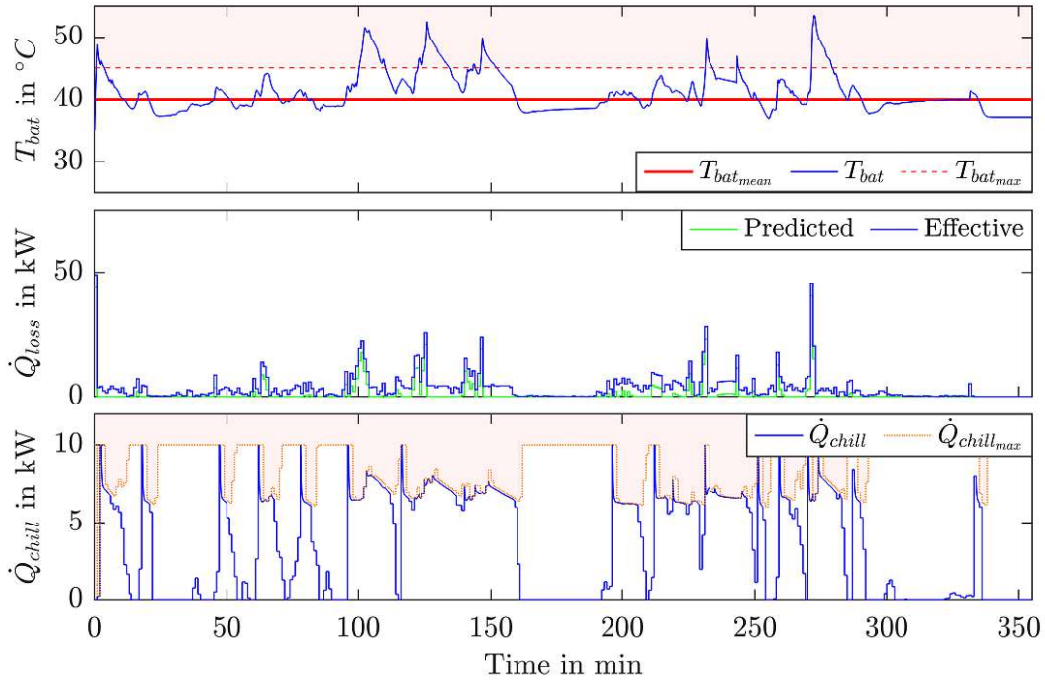

(a) Negative deviation

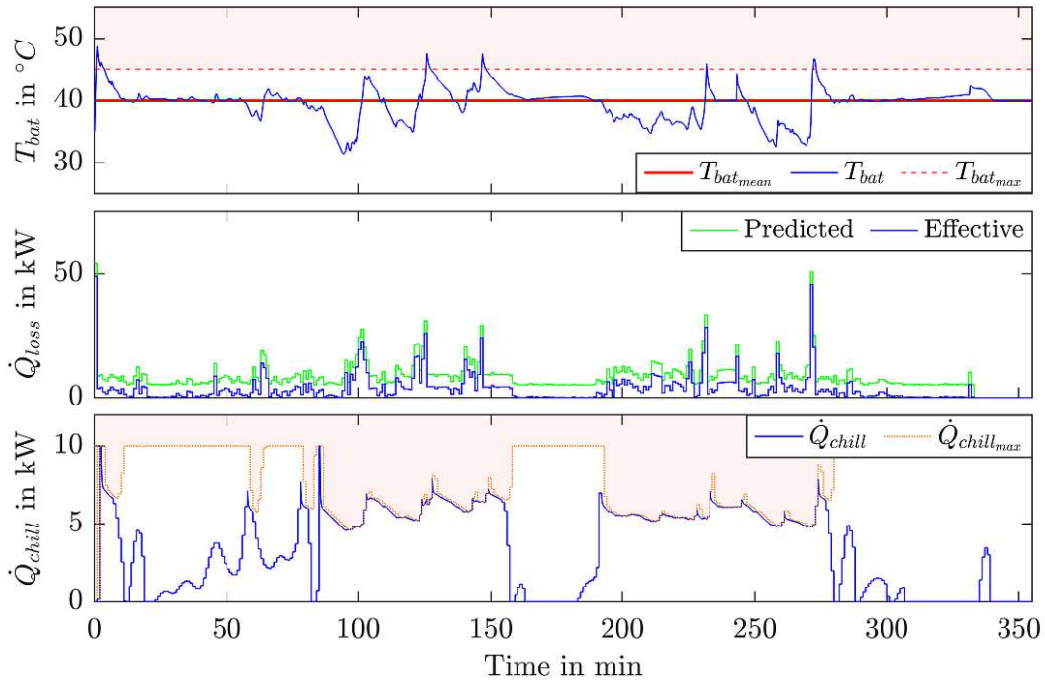

(b) Positive deviation

Figure 3.11: Deviation in the prediction of heat loss $\dot{Q}_{loss}$

SOC, which was seen in Figure 1.8, and therefore is limited in reproducing an exact model. To show a basic example of that deviation, the ohmic losses of the battery were in Figure 3.11

where in Figure 3.11a, the heat loss was underestimated for the whole horizon. That led to exceeding the battery's temperature over the desired limit over the whole horizon. Compared to Figure 3.11b where the ohmic losses on the battery were overestimated and ended up in much stronger precooling that helped them to keep the battery trajectory near the desired temperature of about $40°C$. Summarizing both aspects led to the assumption that it would be overall better to overestimate the battery's ohmic losses to achieve better results on the battery's temperature trajectory.

In addition to these examples of disturbances, many other possibilities have led to miscalculating the system. The entire calculation of a model prediction system relies on the correct prediction of the route profile since the battery's cooling capacity is not strong enough to cool on-site.

Chapter 4

Conclusion

In this thesis, a predictive battery thermal management strategy (BTMS) for heavy-duty fuel cell electric trucks was developed and investigated. The primary goal was to maintain the battery temperature within an optimal range to enhance efficiency and extend battery life under various operational conditions.

Derived from this research, implementing a model predictive control (MPC) system led to significant improvements in maintaining the battery temperature close to the desired reference point. This leads to a reduced thermal stress on the battery and increased the durability and reliability of heavy-duty fuel cell trucks, ultimately leading to lower operational costs and enhanced sustainability. Using route information like elevation and speed limits allows for accurate predictions of electrical loads and cooling needs. This predictive approach helps the system anticipate and counteract thermal issues before they affect battery performance.

The study highlighted the need to optimize the truck's cooling system within its spatial constraints. With limited space for cooling components, it was essential to maximize efficiency. The MPC system achieved this by dynamically adjusting cooling power based on real-time demands.

Simulations of the MPC system with real-world driving cycles confirmed the approach's effectiveness, demonstrating that the predictive thermal management strategy successfully kept battery temperatures within safe limits under various driving conditions. This highlights the strong potential for real-world application and integration into current fuel cell truck systems.

Using a MPC for BTMS is only one step forward for optimizing heavy-duty fuel cell trucks. Implementing an MPC for the energy management system (EMS) could further increase the efficiency of power distribution and thus enhance the cooling strategy. Both concepts, the EMS and BTMS, go hand in hand regarding optimization for hydrogen fuel cell trucks. Real-time data analytics and adaptive control algorithms could improve the responsiveness and accuracy of the predictive thermal management systems.

In conclusion, the predictive BTMS significantly advances heavy-duty fuel cell trucks by maintaining optimal battery temperatures, enhancing performance, and supporting the sustainability of hydrogen fuel cell technology.

Bibliography

[1] Y. Wang, D. F. Ruiz Diaz, K. S. Chen, Z. Wang, and X. C. Adroher, "Materials, technological status, and fundamentals of pem fuel cells – a review," *Materials Today*, vol. 32, pp. 178–203, 2020. [Online]. Available: https://www.sciencedirect.com/science/article/pii/S1369702119304948

[2] M. Brady, "Assessment of battery technology for rail propulsion application," 2017.

[3] ScaniaCVAB, "How does a hydrogen fuel cell electric truck work?" Jan 2020. [Online]. Available: https://www.scania.com/group/en/home/newsroom/news/2020/how-does-a-hydrogen-fuel-cell-electric-truck-work.html

[4] Y. Shen, J. Zhou, J. Zhang, F. Yi, G. Wang, C. Pan, W. Guo, and X. Shu, "Research on energy management of hydrogen fuel cell bus based on deep reinforcement learning considering velocity control," *Sustainability*, vol. 15, no. 16, 2023. [Online]. Available: https://www.mdpi.com/2071-1050/15/16/12488

[5] C. R. Birkl, M. R. Roberts, E. McTurk, P. G. Bruce, and D. A. Howey, "Degradation diagnostics for lithium ion cells," *Journal of Power Sources*, vol. 341, pp. 373–386, 2017. [Online]. Available: https://www.sciencedirect.com/science/article/pii/S0378775316316998

[6] P. E. Ross, "Boeing's battery blues [news]," *IEEE Spectrum*, vol. 50, no. 3, pp. 11–12, 2013.

[7] M. Behrendt, "File:mpc scheme basic.svg." [Online]. Available: https://commons.wikimedia.org/w/index.php?curid=7963069

[8] Qian Wang, Bin Jiang, Bo Li, and Yuying Yan, "A critical review of thermal management models and solutions of lithium-ion batteries for the development of pure electric vehicles," *Renewable and Sustainable Energy Reviews*, vol. 64, pp. 106–128, 2016. [Online]. Available: https://www.sciencedirect.com/science/article/pii/S1364032116301435

[9] D. Wang, Y. Bao, and J. Shi, "Lithium-ion battery internal resistance measurement application in state-of-charge estimation using the extended kalman filter," 2017. [Online]. Available: https://api.semanticscholar.org/CorpusID:28060046

[10] H. Liu, Z. Wei, W. He, and J. Zhao, "Thermal issues about li-ion batteries and recent progress in battery thermal management systems: A review," *Energy Conversion and Management*, vol. 150, pp. 304–330, 2017. [Online]. Available: https://www.sciencedirect.com/science/article/pii/S0196890417307288

[11] S. Arora, "Selection of thermal management system for modular battery packs of electric vehicles: A review of existing and emerging technologies," *Journal of Power Sources*, vol. 400, pp. 621–640, 2018. [Online]. Available: https://www.sciencedirect.com/science/article/pii/S0378775318308796

[12] G. Zhao, X. Wang, M. Negnevitsky, and H. Zhang, "A review of air-cooling battery thermal management systems for electric and hybrid electric vehicles," *Journal of Power Sources*, vol. 501, p. 230001, 2021. [Online]. Available: https://www.sciencedirect.com/science/article/pii/S0378775321005292

[13] K. Chen, Y. Chen, Y. She, M. Song, S. Wang, and L. Chen, "Construction of effective symmetrical air-cooled system for battery thermal management," *Applied Thermal Engineering*, vol. 166, p. 114679, 2020. [Online]. Available: https://www.sciencedirect.com/science/article/pii/S1359431119323312

[14] W. Wu, X. Yang, G. Zhang, X. Ke, Z. Wang, W. Situ, X. Li, and J. Zhang, "An experimental study of thermal management system using copper mesh-enhanced composite phase change materials for power battery pack," *Energy*, vol. 113, pp. 909–916, 2016. [Online]. Available: https://www.sciencedirect.com/science/article/pii/S036054421631043X

[15] W. Zhang, J. Qiu, X. Yin, and D. Wang, "A novel heat pipe assisted separation type battery thermal management system based on phase change material," *Applied Thermal Engineering*, vol. 165, p. 114571, 2020. [Online]. Available: https://www.sciencedirect.com/science/article/pii/S1359431119330960

[16] A. Vezzini, "15 - lithium-ion battery management," in *Lithium-Ion Batteries*, G. Pistoia, Ed. Amsterdam: Elsevier, 2014, pp. 345–360. [Online]. Available: https://www.sciencedirect.com/science/article/pii/B9780444595133000157

[17] D. W. Gao, "Chapter 3 - interfacing between an ess and a microgrid," in *Energy Storage for Sustainable Microgrid*, D. W. Gao, Ed. Oxford: Academic Press, 2015, pp. 79–121. [Online]. Available: https://www.sciencedirect.com/science/article/pii/B9780128033746000032

[18] [Online]. Available: https://www.allegromicro.com/en/applications/automotive/hybrid-electric-48v/battery-management-system#pop-5be1b785-250f-49de-b1b5-798fa3f62d49

[19] M. Islameka, B. A. Budiman, F. B. Juangsa, and M. Aziz, "5 - energy management systems for battery electric vehicles," in *Emerging Trends in Energy Storage Systems and Industrial Applications*, Prabhansu and N. Kumar, Eds. Academic Press, 2023, pp. 113–150. [Online]. Available: https://www.sciencedirect.com/science/article/pii/B9780323905213000065

[20] A. Kampker, H. Heimes, M. Kehrer, S. Hagedorn, P. Reims, and O. Kaul, "Fuel cell system production cost modeling and analysis," *Energy Reports*, vol. 9, pp. 248–255, 2023, 2022 9th International Conference on Power and Energy Systems Engineering. [Online]. Available: https://www.sciencedirect.com/science/article/pii/S2352484722022995

[21] M. de las Nieves Camacho, D. Jurburg, and M. Tanco, "Hydrogen fuel cell heavy-duty trucks: Review of main research topics," *International Journal of Hydrogen Energy*, vol. 47, no. 68, pp. 29 505–29 525, 2022. [Online]. Available: https://www.sciencedirect.com/science/article/pii/S0360319922029068

[22] A. Ferrara, S. Zendegan, H.-M. Koegeler, S. Gopi, M. Huber, J. Pell, and C. Hametner, "Optimal calibration of an adaptive and predictive energy management strategy for fuel cell electric trucks," *Energies*, vol. 15, no. 7, 2022. [Online]. Available: https://www.mdpi.com/1996-1073/15/7/2394

[23] A. Ferrara, M. Okoli, S. Jakubek, and C. Hametner, "Energy management of heavy-duty fuel cell electric vehicles: Model predictive control for fuel consumption and lifetime optimization," *IFAC-PapersOnLine*, vol. 53, no. 2, pp. 14 205–14 210, 2020, 21st IFAC World Congress. [Online]. Available: https://www.sciencedirect.com/science/article/pii/S2405896320314233

[24] R. MATULKA, "The history of the electric car." [Online]. Available: https://www.energy.gov/articles/history-electric-car

[25] T. Lang, "130 jahre elektroautos: Kurze blüte, langer flopp," Aug 2012. [Online]. Available: https://web.archive.org/web/20130613062747/http://auto-presse.de/autonews.php?newsid=137630

[26] R. Wang, C. Song, W. Huang, and J. Zhao, "Improvement of battery pack efficiency and battery equalization based on the extremum seeking control," *International Journal of Electrical Power and Energy Systems*, vol. 137, p. 107829, 2022. [Online]. Available: https://www.sciencedirect.com/science/article/pii/S0142061521010450

[27] S. I. AL-Saedi, A. J. Haider, A. N. Naje, and N. Bassil, "Improvement of li-ion batteries energy storage by graphene additive," *Energy Reports*, vol. 6, pp. 64–71, 2020, technologies and Materials for Renewable Energy, Environment and Sustainability. [Online]. Available: https://www.sciencedirect.com/science/article/pii/S2352484719308637

[28] T. ming Gao, N. Fan, W. Chen, and T. Dai, "Lithium extraction from hard rock lithium ores (spodumene, lepidolite, zinnwaldite, petalite): Technology, resources, environment and cost," *China Geology*, vol. 6, no. 1, pp. 137–153, 2023. [Online]. Available: https://www.sciencedirect.com/science/article/pii/S2096519223008601

[29] M. Pagliaro and F. Meneguzzo, "Lithium battery reusing and recycling: A circular economy insight," *Heliyon*, vol. 5, no. 6, p. e01866, 2019. [Online]. Available: https://www.sciencedirect.com/science/article/pii/S2405844019347012

[30] M. Chen, X. Ma, B. Chen, R. Arsenault, P. Karlson, N. Simon, and Y. Wang, "Recycling end-of-life electric vehicle lithium-ion batteries," *Joule*, vol. 3, no. 11, pp. 2622–2646, 2019. [Online]. Available: https://www.sciencedirect.com/science/article/pii/S254243511930474X

[31] G. Senthamaraikkannan, D. Chakrabarti, and V. Prasad, "Chapter 13 - transport fuel – lng and methane," in *Future Energy (Second Edition)*, second edition ed., T. M. Letcher, Ed. Boston: Elsevier, 2014, pp. 271–288. [Online]. Available: https://www.sciencedirect.com/science/article/pii/B9780080994246000132

[32] R. Gantner, "Der vergleich: Batterie (bev) oder brennstoffzelle (fcev) im fahrzeug," May 2023. [Online]. Available: https://www.all-electronics.de/e-mobility/bev-oder-fcev-batterie-oder-brennstoffzelle-im-fahrzeug-554.html

[33] L. Schwichtenberg, "Wasserstoff ist tot: Honda plant 30 neue elektro-modelle." [Online]. Available: https://efahrer.chip.de/news/wasserstoff-ist-tot-honda-plant-30-neue-elektro-modelle_107757

[34] ScaniaCVAB, "Scania to deliver fuel cell trucks to switzerland," Nov 2022. [Online]. Available: https://www.scania.com/group/en/home/newsroom/news/2022/scania-to-deliver-fuel-cell-trucks-to-switzerland.html

[35] W. Gomoll, "Willkommen auf golem.de!" Mar 2023. [Online]. Available: https://www.golem.de/news/fahrbericht-nikola-tre-fcev-der-wasserstoff-lkw-mit-mobiler-zapfsaeule-2303-172621.html

[36] A. Olabi, H. M. Maghrabie, O. H. K. Adhari, E. T. Sayed, B. A. Yousef, T. Salameh, M. Kamil, and M. A. Abdelkareem, "Battery thermal management systems: Recent progress and challenges," *International Journal of Thermofluids*, vol. 15, p. 100171, 2022. [Online]. Available: https://www.sciencedirect.com/science/article/pii/S2666202722000350

[37] J. Chastain, J. Wagner, and J. Eberth, "Advanced engine cooling – components, testing and observations," *IFAC Proceedings Volumes*, vol. 43, no. 7, pp. 294–299, 2010, 6th IFAC Symposium on Advances in Automotive Control. [Online]. Available: https://www.sciencedirect.com/science/article/pii/S1474667015368440

[38] M. Lu, X. Zhang, J. Ji, X. Xu, and Y. Zhang, "Research progress on power battery cooling technology for electric vehicles," *Journal of Energy Storage*, vol. 27, p. 101155, 2020. [Online]. Available: https://www.sciencedirect.com/science/article/pii/S2352152X19311193

[39] Y. Fan, Y. Bao, C. Ling, Y. Chu, X. Tan, and S. Yang, "Experimental study on the thermal management performance of air cooling for high energy density cylindrical lithium-ion batteries," *Applied Thermal Engineering*, vol. 155, pp. 96–109, 2019. [Online]. Available: https://www.sciencedirect.com/science/article/pii/S1359431118376695

[40] T. Wang, K. Tseng, J. Zhao, and Z. Wei, "Thermal investigation of lithium-ion battery module with different cell arrangement structures and forced air-cooling strategies," *Applied Energy*, vol. 134, pp. 229–238, 2014. [Online]. Available: https://www.sciencedirect.com/science/article/pii/S0306261914008162

[41] M. Ye, Y. Xu, and Y. Huangfu, "The structure optimization of lithium-ion battery pack based on fluid-solid conjugate thermodynamic analysis," *Energy Procedia*, vol. 152, pp. 643–648, 2018, cleaner Energy for Cleaner Cities. [Online]. Available: https://www.sciencedirect.com/science/article/pii/S1876610218307690

[42] D. C. Erb, S. Kumar, S. E. Sarma, and E. Carlson, "Size matters: Why cell size is vital for minimizing cost of air-cooling in battery packs," in *2015 IEEE Transportation Electrification Conference and Expo (ITEC)*, 2015, pp. 1–6.

[43] Z. Rao, Y. Huo, X. Liu, and G. Zhang, "Experimental investigation of battery thermal management system for electric vehicle based on paraffin/copper foam," *Journal of the Energy Institute*, vol. 88, no. 3, pp. 241–246, 2015. [Online]. Available: https://www.sciencedirect.com/science/article/pii/S1743967114202030

[44] A. Hussain, C. Tso, and C. Y. Chao, "Experimental investigation of a passive thermal management system for high-powered lithium ion batteries using nickel foam-paraffin composite," *Energy*, vol. 115, pp. 209–218, 2016. [Online]. Available: https://www.sciencedirect.com/science/article/pii/S0360544216312488

[45] M. Alipanah and X. Li, "Numerical studies of lithium-ion battery thermal management systems using phase change materials and metal foams," *International Journal*

of Heat and Mass Transfer, vol. 102, pp. 1159–1168, 2016. [Online]. Available: https://www.sciencedirect.com/science/article/pii/S0017931016312388

[46] J. Zhao, P. Lv, and Z. Rao, "Experimental study on the thermal management performance of phase change material coupled with heat pipe for cylindrical power battery pack," *Experimental Thermal and Fluid Science*, vol. 82, pp. 182–188, 2017. [Online]. Available: https://www.sciencedirect.com/science/article/pii/S0894177716303338

[47] H. Fathabadi, "High thermal performance lithium-ion battery pack including hybrid active–passive thermal management system for using in hybrid/electric vehicles," *Energy*, vol. 70, pp. 529–538, 2014. [Online]. Available: https://www.sciencedirect.com/science/article/pii/S0360544214004599

[48] S. Cheng, C. Fang, L. Xu, J. Li, and M. Ouyang, "Model-based temperature regulation of a pem fuel cell system on a city bus," *International Journal of Hydrogen Energy*, vol. 40, no. 39, pp. 13 566–13 575, 2015. [Online]. Available: https://www.sciencedirect.com/science/article/pii/S0360319915021382

[49] S. Melançon, "Ev battery cooling: Challenges and solutions," Apr 2022. [Online]. Available: https://www.laserax.com/blog/ev-battery-cooling

[50] Y. Huang, S. Wang, Y. Lu, R. Huang, and X. Yu, "Study on a liquid cooled battery thermal management system pertaining to the transient regime," *Applied Thermal Engineering*, vol. 180, p. 115793, 2020. [Online]. Available: https://www.sciencedirect.com/science/article/pii/S1359431120332750

[51] M. Larrañaga-Ezeiza, G. Vertiz Navarro, I. Galarza Garmendia, P. Fernandez Arroiabe, M. Martinez-Aguirre, and J. Berasategi Arostegui, "Parametric optimisation of a direct liquid cooling based prototype for electric vehicles focused on pouch-type battery cells," *World Electric Vehicle Journal*, vol. 13, no. 8, 2022. [Online]. Available: https://www.mdpi.com/2032-6653/13/8/149

[52] M. Larrañaga-Ezeiza, G. Vertiz, P. Arroiabe, M. Martinez-Agirre, and J. Berasategi, "A novel direct liquid cooling strategy for electric vehicles focused on pouch type battery cells," *Applied Thermal Engineering*, vol. 216, p. 118869, 2022. [Online]. Available: https://www.sciencedirect.com/science/article/pii/S1359431122008080

[53] Y. Ding, H. Ji, M. Wei, and R. Liu, "Effect of liquid cooling system structure on lithium-ion battery pack temperature fields," *International Journal of Heat and Mass Transfer*, vol. 183, p. 122178, 2022. [Online]. Available: https://www.sciencedirect.com/science/article/pii/S0017931021012771

[54] J. Zhao, Z. Rao, and Y. Li, "Thermal performance of mini-channel liquid cooled cylinder based battery thermal management for cylindrical lithium-ion power battery," *Energy Conversion and Management*, vol. 103, pp. 157–165, 2015. [Online]. Available: https://www.sciencedirect.com/science/article/pii/S019689041500597X

[55] C. Zhao, W. Cao, T. Dong, and F. Jiang, "Thermal behavior study of discharging/charging cylindrical lithium-ion battery module cooled by channeled liquid flow," *International Journal of Heat and Mass Transfer*, vol. 120, pp. 751–762, 2018. [Online]. Available: https://www.sciencedirect.com/science/article/pii/S0017931017337948

[56] J. Cao, M. Luo, X. Fang, Z. Ling, and Z. Zhang, "Liquid cooling with phase change materials for cylindrical li-ion batteries: An experimental and numerical study," *Energy*, vol. 191, p. 116565, 2020. [Online]. Available: https://www.sciencedirect.com/science/article/pii/S0360544219322601

[57] T. Amalesh and N. Lakshmi Narasimhan, "Liquid cooling vs hybrid cooling for fast charging lithium-ion batteries: A comparative numerical study," *Applied Thermal Engineering*, vol. 208, p. 118226, 2022. [Online]. Available: https://www.sciencedirect.com/science/article/pii/S1359431122001880

[58] A. Quiroz, "What is energy management system and electric vehicle energy management system," May 2022. [Online]. Available: https://blog.intellimeter.com/what-is-energy-management-system-and-electric-vehicle-energy-management-system

[59] A. Lahnaoui, C. Wulf, H. Heinrichs, and D. Dalmazzone, "Optimizing hydrogen transportation system for mobility via compressed hydrogen trucks," *International Journal of Hydrogen Energy*, vol. 44, no. 35, pp. 19 302–19 312, 2019, a Special Issue with the Papers Selected from the 7th World Hydrogen Technologies Convention. [Online]. Available: https://www.sciencedirect.com/science/article/pii/S0360319918335171

[60] M. Aminudin, S. Kamarudin, B. Lim, E. Majilan, M. Masdar, and N. Shaari, "An overview: Current progress on hydrogen fuel cell vehicles," *International Journal of Hydrogen Energy*, vol. 48, no. 11, pp. 4371–4388, 2023. [Online]. Available: https://www.sciencedirect.com/science/article/pii/S0360319922048534

[61] L. Wang, *Model predictive control system design and implementation using MATLAB*, ser. Advances in industrial control. London and Heidelberg: Springer, 2009.